Title

Nitric oxide synthase and reduced arterial tone contribute to arteriovenous malformation

Journal

Science Advances, 9(21)

ISSN

2375-2548

Authors

Huang, Lawrence

Cheng, Feng

Zhang, Xuetao

et al.

Publication Date

2023-05-26

DOI

10.1126/sciadv.ade7280

DEVELOPMENTAL BIOLOGY

Nitric oxide synthase and reduced arterial tone contribute to arteriovenous malformation

Lawrence Huang[1]†, Feng Cheng[1]†‡, Xuetao Zhang[1], Jacek Zielonka[2], Matthew A. Nystoriak[3]§, Weiwei Xiang[1], Kunal Raygor[1], Shaoxun Wang[1], Aditya Lakshmanan[1], Weiya Jiang[1], Sai Yuan[1], Kevin S. Hou[1], Jiayi Zhang[1], Xitao Wang[1], Arsalan U. Syed[3], Matea Juric[2], Takamune Takahashi[4], Manuel F. Navedo[3], Rong A. Wang[1]*

Mechanisms underlying arteriovenous malformations (AVMs) are poorly understood. Using mice with endothelial cell (EC) expression of constitutively active Notch4 (Notch4*^{EC}), we show decreased arteriolar tone in vivo during brain AVM initiation. Reduced vascular tone is a primary effect of Notch4*^{EC}, as isolated pial arteries from asymptomatic mice exhibited reduced pressure-induced arterial tone ex vivo. The nitric oxide (NO) synthase (NOS) inhibitor NG-nitro-L-arginine (L-NNA) corrected vascular tone defects in both assays. L-NNA treatment or endothelial NOS (*eNOS*) gene deletion, either globally or specifically in ECs, attenuated AVM initiation, assessed by decreased AVM diameter and delayed time to moribund. Administering nitroxide antioxidant 4-hydroxy-2,2,6,6-tetramethylpiperidine-1-oxyl also attenuated AVM initiation. Increased NOS-dependent production of hydrogen peroxide, but not NO, superoxide, or peroxynitrite was detected in isolated Notch4*^{EC} brain vessels during AVM initiation. Our data suggest that eNOS is involved in Notch4*^{EC}-mediated AVM formation by up-regulating hydrogen peroxide and reducing vascular tone, thereby permitting AVM initiation and progression.

INTRODUCTION

Arteriovenous (AV) malformations (AVMs) are devastating high-flow vascular anomalies that shunt blood directly from arteries to veins by displacing intervening capillaries, capable of causing both hemorrhage and ischemia (*1*, *2*). Developing better therapeutic interventions requires an improved understanding of the mechanisms underlying AVM pathogenesis.

Recent reports demonstrate that Notch signaling, including Notch1 and Notch4, is aberrantly increased in human brain AVMs (*3*–*5*). Notch4 gene polymorphisms are also potential risk factors for human brain AVMs (*6*). Downstream of Notch signaling, loss-of-function mutations in ephrin type-B receptor 4 (EphB4) have been implicated in human AVM in a form of capillary malformation–AVM (*7*). Expression of mutant KRAS in cultured endothelial cells (ECs) induced up-regulation of Notch pathway genes, such as Notch1, Dll4, Jag1, and Jag2, thus linking Notch signaling to KRAS mutation–induced human brain AVM (*8*). Furthermore, Notch signaling interacts with activin receptor–like kinase 1 signaling, whose haploinsufficiency leads to hereditary hemorrhagic telangiectasia (HHT), a human vascular disorder that is characterized by AVMs (*9*). These findings suggest that Notch signaling is involved in human AVM pathogenesis.

Postnatal perturbation of Notch signaling, a master regulator of AV specification, leads to AVMs in mice (*10*–*15*). Notch receptors (Notch1 and Notch4) and ligands (Dll1, Dll4, Jag1, and Jag2) are expressed in arterial but not venous ECs (*16*, *17*). Notch determines arterial EC fate by promoting the expression of arterial molecular markers while suppressing the expression of venous molecular markers (*18*). Our previous comparative studies show that constitutively active Notch1 and constitutively active Notch4 both induce AVMs (*13*). While Notch1 is expressed in many tissues, Notch4 is more restricted to the endothelium. Therefore, we focused on the role and mechanisms of Notch4 in AVM formation. We show that endothelial-specific expression of constitutively active Notch4 (Notch4*; Notch4*^{EC} herein), induces AVMs with 100% penetrance in mice (*10*, *12*, *14*).

The degree of constriction and dilation of small-diameter arteries and arterioles is a key determinant of capillary perfusion pressure and blood flow (*19*). Accordingly, it is plausible that impaired regulation of vascular tone in resistance arteries contributes to capillary enlargement and flow-perpetuated AV shunt growth. Thus, to understand the mechanisms by which Notch4*^{EC} elicits AVMs, we hypothesize that vascular tone (e.g., pressure-induced constriction) (*20*) is compromised in Notch4*^{EC} mice, contributing to AVM formation by disrupting normal vasoconstriction. Because the endothelial nitric oxide (NO) synthase (NOS) (eNOS) pathway is a critical modulator of vascular function, including resting arterial tone and cerebral blood flow (*21*–*23*), we tested the role of eNOS in modulating AVM formation in Notch4*^{EC} mice.

[1]Laboratory for Accelerated Vascular Research, Department of Surgery, University of California San Francisco, San Francisco, CA 94143, USA. [2]Free Radical Research Laboratory, Department of Biophysics, Medical College of Wisconsin, Milwaukee, WI 53226, USA. [3]Department of Pharmacology, University of California, Davis, Davis, CA 95616, USA. [4]Division of Nephrology and Hypertension, Vanderbilt University Medical Center, Nashville, TN 37232, USA.
*Corresponding author. Email: rong.wang@ucsf.edu
†These authors contributed equally to this work.
‡Present address: Center for Cancer and Immunology Research, Children's National Research Institute, Children's National Hospital, Washington, DC 20010, USA.
§Present address: Division of Cardiovascular Medicine, Department of Medicine, University of Louisville, Louisville, KY 40202, USA.

RESULTS

Mice expressing Notch4* in ECs exhibited impaired cerebral vascular tone

To test whether the expression of Notch4* in ECs affects cerebrovascular tone in vivo, we used our mouse model carrying *Tie2-tTA;TRE-Notch4** transgenes, in which Notch4* is specifically expressed in ECs (i.e., Notch4*^{EC} mice) (*10*). We measured diameters of arterial branches of the middle and anterior cerebral arteries (*24*) and their first-order arterioles through an open cranial window in anesthetized postnatal day 16 (P16) Notch4*^{EC} (in which Notch4*^{EC} expression was turned on from birth) and *Tie2-tTA* control mice. We measured vessel diameters at baseline with topical administration of artificial cerebrospinal fluid (aCSF) and at a maximally dilated state with aCSF devoid of Ca^{2+} and containing 1 μM of the L-type Ca^{2+} channel antagonist nifedipine (0 Ca^{2+} aCSF + nifedipine) using our established procedures (Fig. 1A) (*24*). We verified the in vivo assay in genetic control mice by showing the known inverse correlation between vessel diameter and tone (fig. S1) and detected a statistically significant reduction in arteriolar tone in Notch4*^{EC} versus control mice (Fig. 1B).

To verify the manual quantification, we implemented a computational unbiased edge detection method for quantifying vessel diameter (fig. S2). Comparative analysis between edge detection and manual measurements showed a positive linear correlation in measured diameters and tone (fig. S3). Using this method, we confirmed the reduction in arteriolar tone in Notch4*^{EC} versus control mice (Fig. 1C). We also measured vasodilation in response to acetylcholine (ACh) and did not detect a statistically significant change in ACh-induced vasodilation in Notch4*^{EC} arteries or arterioles compared to those of controls (fig. S4). These data indicate that cerebrovascular tone is suppressed in mice with constitutively active endothelial Notch4.

We further assessed pressure-induced arterial tone on intact cerebral arteries isolated from 5- to 6-week-old Notch4*^{EC} mice, in

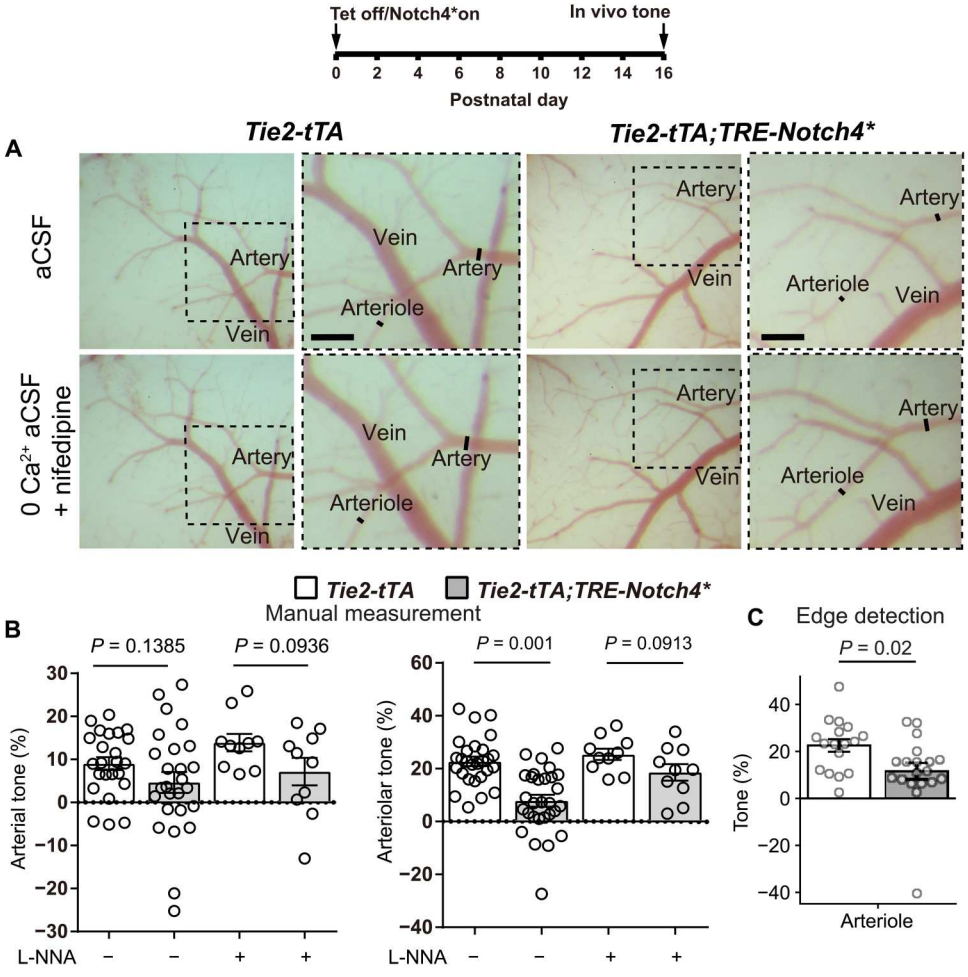

Fig. 1. Impaired in vivo cerebral vascular tone in mice expressing Notch4* in ECs. (**A**) Representative images of middle cerebral and anterior cerebral arteries and branches in live postnatal day 16 (P16) *Tie2-tTA* and *Tie2-tTA;TRE-Notch4** mice visualized through an open cranial window. Scale bars, 150 μm. aCSF, artificial cerebrospinal fluid. (**B**) Arterial and arteriolar tone in the absence (−) and presence (+) of NG-nitro-L-arginine (L-NNA) treatment (30 mg/kg) (percentage change from maximum passive diameter). (In the absence of L-NNA, artery: *Tie2-tTA*, $n = 24$ mice; *Tie2-tTA;TRE-Notch4**, $n = 27$ mice; $P = 0.1385$, *t* test; arteriole: *Tie2-tTA*, $n = 27$ mice; *Tie2-tTA;TRE-Notch4**, $n = 29$ mice; $P = 0.001$, *t* test.) (In the presence of L-NNA, artery: *Tie2-tTA*, $n = 10$ mice; *Tie2-tTA;TRE-Notch4**, $n = 10$ mice; $P = 0.0936$, *t* test; arteriole: *Tie2-tTA*, $n = 10$ mice; *Tie2-tTA;TRE-Notch4**, $n = 10$ mice; $P = 0.913$, *t* test.) (**C**) Arteriolar tone by edge detection from line profiles (*Tie2-tTA*, $n = 17$ mice; *Tie2-tTA;TRE-Notch4**, $n = 19$ mice; $P = 0.02$, *t* test).

which Notch4*^{EC} expression was induced for 10 days. Note that these adult Notch4*^{EC} mice did not exhibit brain AVMs (*10*), and we therefore provide a model to assess the primary effect of Notch4*^{EC} on arterial tone in the absence of confounding factors associated with the presence of AVMs. Pressure-dependent vasoconstriction was observed in control arteries but was nearly abolished in Notch4*^{EC} arteries (Fig. 2, A and B). We tested whether vasoconstriction in response to direct membrane depolarization and activation of voltage-dependent calcium channels was affected in arteries from Notch4*^{EC} mice (*20*). This response was similar between groups, suggesting that loss of tone was not due to reduced Ca^{2+}-dependent smooth muscle contractile function (fig. S5). To assess the role of NOS, we tested whether the loss of vascular tone in Notch4*^{EC} arteries was sensitive to the NOS inhibitor NG-nitro-L-arginine (L-NNA). Consistent with this, Notch4*^{EC} arteries exhibited a greater degree of vasoconstriction in response to L-NNA compared to control arteries (Fig. 2, C and D), such that no differences in tone were observed in the presence of L-NNA (Fig. 2E). On the basis of the results of ex vivo arterial diameter experiments, we determined whether NOS activity underlies the loss of arteriolar tone in vivo. Whereas Notch4*^{EC} mice had reduced arteriolar tone relative to control mice, these differences were abolished in the presence of L-NNA (Fig. 1B). These data suggest that endothelial Notch4* suppresses small-diameter cerebrovascular tone via the enhanced activity of NOS.

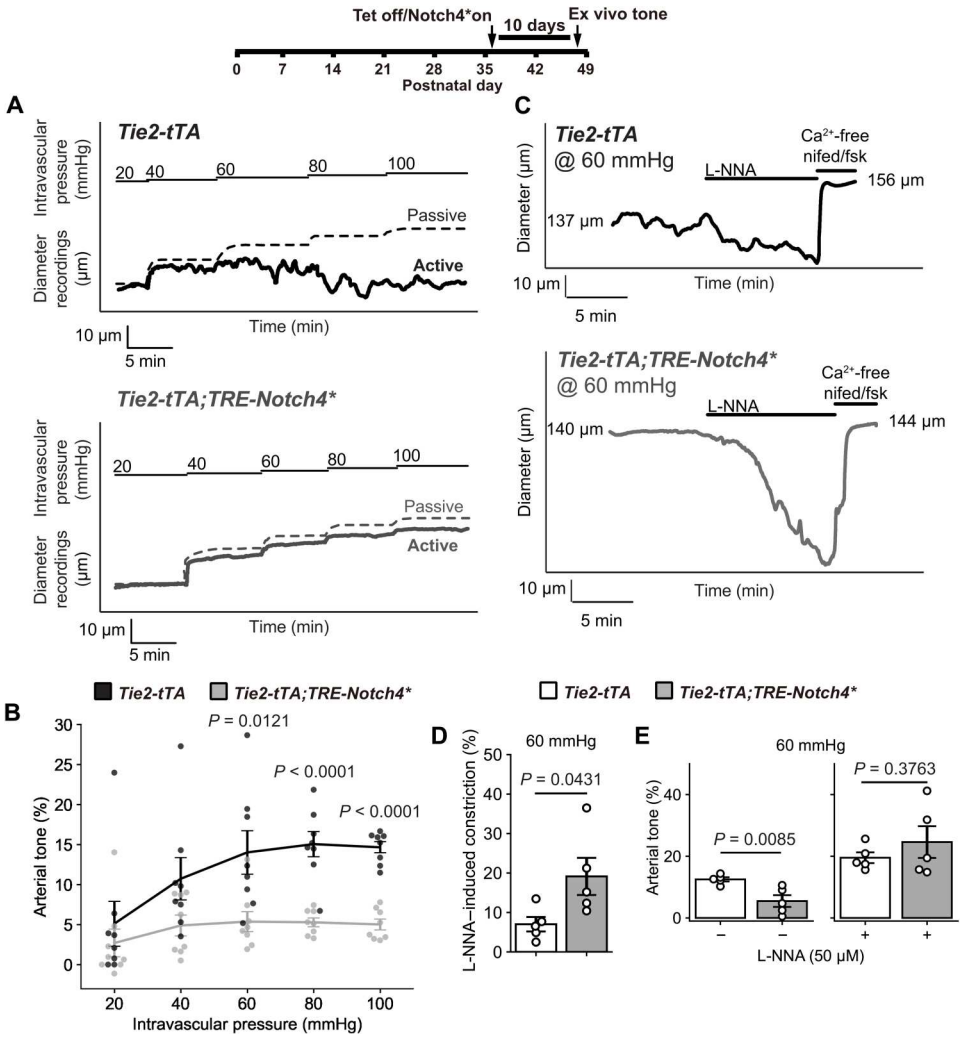

Fig. 2. Impaired ex vivo cerebral vascular tone in mice expressing Notch4* in ECs. (**A**) Representative diameter recordings from pressurized *Tie2-tTA* and *Tie2-tTA;TRE-Notch4** cerebral arteries over a range of intravascular pressures. Solid and dashed lines indicate active and passive diameters, respectively. (**B**) Arterial tone (percentage change from maximum passive diameter) measured in isolated cerebral arteries over a range of intravascular pressures. ($n = 8$ arteries from seven mice per group; *Tie2-tTA* versus *Tie2-tTA;TRE-Notch4** at 20 mmHg, $P = 0.4783$; 40 mmHg, $P = 0.0667$; 60 mmHg, $P = 0.0121$; 80 and 100 mmHg, $P < 0.0001$, *t* test). (**C**) Representative diameter recordings from pressurized (60 mmHg) cerebral arteries in the absence and presence of 50 μM L-NNA. The maximum passive diameter was recorded at the end of the experiment in Ca2+-free perfusate containing nifedipine (nifed; 1 μM) and forskolin (fsk; 0.5 μμ). (**D**) L-NNA–induced constriction (percentage change in diameter normalized to maximum passive diameter for vessels shown in (D). ($n = 5$ arteries from four mice per group; $P = 0.0431$, *t* test.) (**E**) Arterial tone at 60 mmHg of intravascular pressure in the absence (–) and presence (+) of 50 μM L-NNA ($n = 5$ arteries from four mice per group; *Tie2-tTA* versus *Tie2-tTA;TRE-Notch4** in the absence of L-NNA, $P = 0.0085$; in the presence of L-NNA, $P = 0.3763$, *t* test). Error bars, SEM.

Mosaic Notch4* expression in ECs was sufficient to reduce vascular tone and initiate brain AVMs

Because somatic mutations, often mosaic, are found in human brain AVMs, we tested whether Notch4* expression was mosaic in our Notch4*^{EC} brain AVM mouse model. The transgenic Notch4* does not contain an extracellular domain and does not require ligand binding to signal, but rather it is constitutively cleaved and translocated into the nucleus, thus presenting a nuclear staining pattern. We detected nuclear Notch4* using an antibody to the cytoplasmic domain of the Notch4 receptor. This antibody, in principle, should also recognize the endogenous Notch4, but because the endogenous Notch4 is expressed at lower levels and not concentrated in the nucleus, it is not detected by this antibody. Accordingly, this antibody practically detects only transgenic Notch4*. We identified individual Notch4*-positive ECs in arteries, veins, and capillaries, using double staining for Notch4* and vascular endothelial (VE)–cadherin, which highlights EC boundaries. We measured the fluorescence intensity of Notch4* immunostaining (Notch4 intracellular domain; Notch4ICD) in EC nuclei in P12 cortexes (fig. S6A), when enlargement of capillary-like vessels become apparent in Notch4*^{EC} mice (*13*). We found that ~60% of ECs were Notch4* positive and evenly distributed throughout arteries, veins, and capillaries in Notch4*^{EC} mice (fig. S6B), without obvious difference in Notch4* intensity in individual ECs from arteries, veins, and capillaries (fig. S6C). As a control, Notch4ICD was not detected in brain blood vessels of *Tie2-tTA* mice (fig. S6A).

L-NNA decreased AVM diameter in brains of mice expressing Notch4* in ECs

To evaluate the effects of pharmacological inhibition of NOS on Notch4*^{EC}-mediated brain AVM, we examined tomato lectin–perfused whole-mount brain preparations of Notch4*^{EC} mice. Notch4*^{EC} expression was induced at birth by withdrawing tetracycline treatment. Notch4*^{EC} mice along with genetic control mice (carrying *Tie2-tTA*) were treated with saline or L-NNA daily starting from P1, and AV connection diameters were measured at their narrowest point at P24 (or at moribund if mice became moribund earlier than P24; Fig. 3A; see Materials and Methods for assessing moribundity). By P24, all Notch4*^{EC} mice are expected to have developed enlarged AV connections with a diameter of ≥12.5 μm, while connections of this diameter are not observed in control mice after P12 (*13*). Accordingly, enlarged AV connections were widespread in saline-treated Notch4*^{EC} mice at P24. While NOS inhibition by L-NNA treatment did not completely prevent brain AVM initiation, as AV shunts, ≥12.5 μm remained (Fig. 3A and fig. S7), AV connection diameter was smaller in L-NNA–treated Notch4*^{EC} mice at P24 (14 ± 2 μm) compared to saline-treated Notch4*^{EC} mice (30 ± 2 μm; Fig. 3B). L-NNA–treated Notch4*^{EC} mice exhibited a smaller fraction (1 ± 1%) of severely enlarged AV connections with a diameter ≥ 30 μm compared to that in saline-treated Notch4*^{EC} mice (44 ± 5%; Fig. 3C).

To determine whether NOS inhibition affected brain AVM initiation, Notch4*^{EC} and genetic control mice were treated with saline or L-NNA daily starting on P1, and AV connection diameters were measured at P12, when vessel enlargement become apparent in Notch4*^{EC} mice (*13*). At P12, AV connection diameter in L-NNA–treated Notch4*^{EC} mice (6 ± 1 μm) was smaller compared to that in saline-treated Notch4*^{EC} mice (15 ± 1 μm) and was not statistically different from that in saline- (5 ± 0.2 μm) or L-NNA–treated genetic controls (5 ± 0.1 μm) (Fig. 3, D and E). In addition, L-NNA–treated Notch4*^{EC} mice exhibited a smaller fraction (2 ± 2%) of enlarged AV connections with a diameter of ≥12.5 μm compared to that in saline-treated Notch4*^{EC} mice (56 ± 4%; Fig. 3F). These data suggest that L-NNA treatment attenuated AVM initiation at P12. Together, our data at P24 and P12 suggest that NOS inhibition by L-NNA treatment attenuated the initiation and delayed the progression of brain AVM in Notch4*^{EC} mice. Next, we investigated whether L-NNA treatment can reverse established AVMs. Saline or L-NNA was injected daily starting from P16, when AVMs are established, and AV connection diameters were measured at P24, when a majority of the mice got ill. The AV connection diameter in L-NNA–treated Notch4*^{EC} mice (30 ± 4 μm), although slightly reduced, was not statistically different than from saline-treated Notch4*^{EC} mice (34 ± 2 μm; fig. S8), suggesting that L-NNA treatment could not reverse established AVMs.

L-NNA treatment decreased AVM diameter in brains of moribund mice expressing Notch4* in ECs

To assess the full effect of NOS inhibition on brain AVM formation in Notch4*^{EC} mice, we evaluated the mice at the moribund stage. We used immunostaining of VE-cadherin, because it did not require perfusion and could be performed on moribund mice that were too weak to be perfused sufficiently. Expression of VE-cadherin showed that moribund L-NNA–treated Notch4*^{EC} mice exhibited a less severe AVM phenotype compared to moribund saline-treated Notch4*^{EC} mice (fig. S9A), with decreased AV connection diameter (19 ± 2 μm + L-NNA versus 30 ± 4 μm + saline) and smaller fraction of severely enlarged AV connections with a diameter of ≥30 μm over total AV connections quantified (14 ± 6% + L-NNA versus 44 ± 10% + saline), despite being harvested at older ages (fig. S9, C to E). Genetic controls without Notch4*^{EC} expression treated daily with saline or L-NNA exhibited no gross vascular phenotype after 40 or 50 days, respectively (fig. S9, B and C). These results suggest that L-NNA–mediated attenuation of Notch4*^{EC} brain AVM persisted until the late stages of disease progression.

L-NNA treatment delayed illness progression in mice expressing Notch4* in ECs

In our Notch4*^{EC} brain AVM model, Notch4*^{EC} activation from birth leads to death by 5 weeks of age (*14*). Because L-NNA treatment attenuated vessel enlargement, we evaluated its effect on disease outcome. Administering L-NNA daily delayed but did not prevent illness in Notch4*^{EC} mice (median moribund age: P30 + L-NNA versus P25 + saline; Fig. 4A). Saline- or L-NNA–treated genetic controls without Notch4*^{EC} expression did not result in illness or moribundity during this time window. These results suggest that decreased brain AV connection diameter in L-NNA–treated Notch4*^{EC} mice was accompanied by delayed illness progression.

AVM formation in Notch4*^{EC} mice is widespread and not limited to the brain (*10*, *12*). We previously demonstrated that one compensatory response to peripheral AV shunting was cardiomegaly (*10*). To assess whether Notch4*^{EC}-associated heart enlargement was affected following NOS inhibition, we measured heart-to-body weight ratio at P24, when enlarged brain AV connections were readily detected. Heart-to-body weight ratio in Notch4*^{EC} mice was lower when treated with L-NNA compared to saline treatment (Fig. 4B). These results provide further evidence that inhibiting

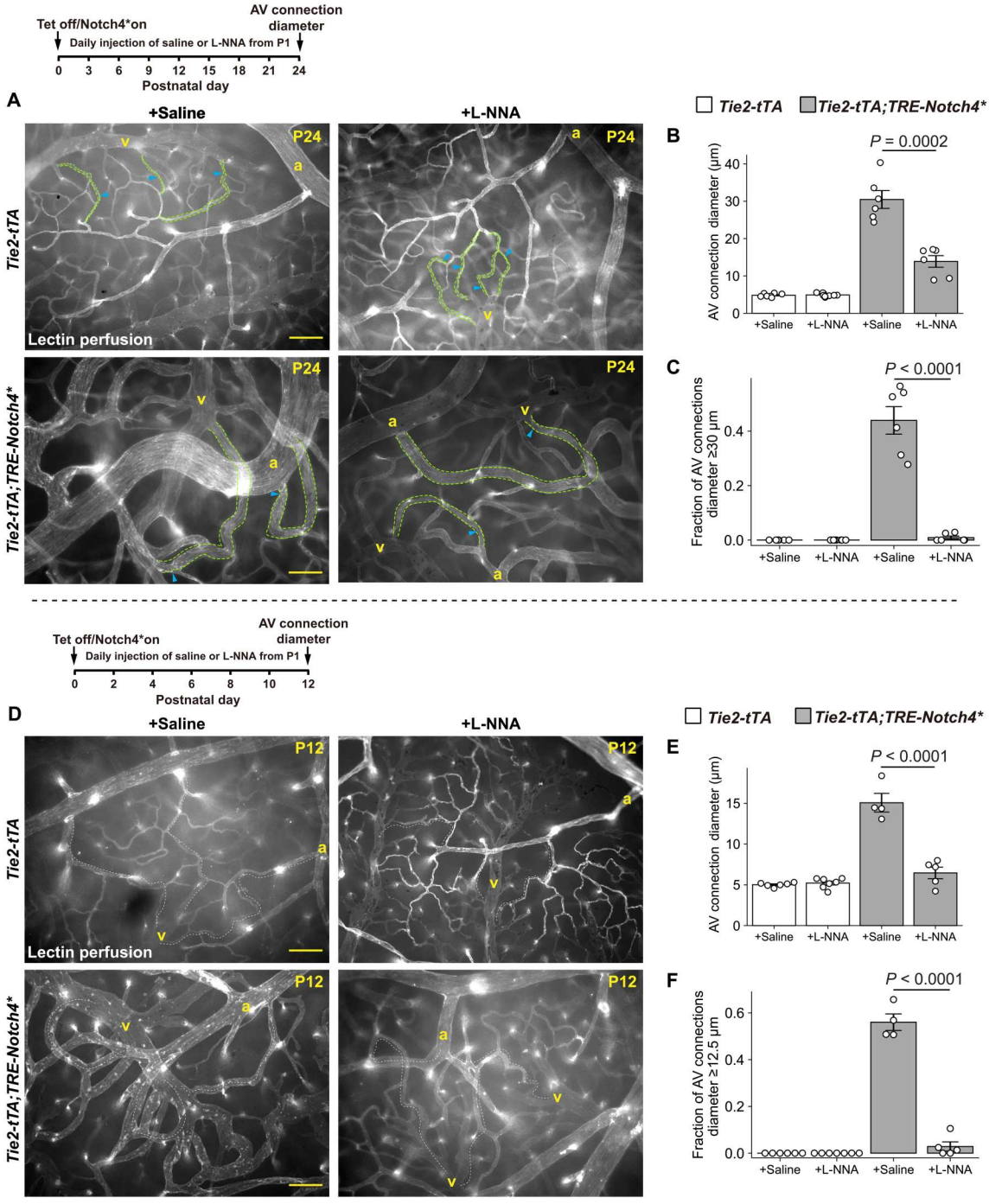

Fig. 3. L-NNA decreased AVM diameter in brains of mice expressing Notch4* in ECs. (**A**) Lectin-perfused vasculature on P24 surface cerebral cortex of *Tie2-tTA* and *Tie2-tTA;TRE-Notch4** mice treated with saline or L-NNA (a, artery; v, vein; dashed lines, example AV connections; arrowheads, example points of measurement for AV connection diameter; scale bars, 100 μm). (**B**) Arteriovenous (AV) connection diameter (*Tie2-tTA* + saline, $n = 7$ mice; *Tie2-tTA* + L-NNA, $n = 9$ mice; *Tie2-tTA;TRE-Notch4** + saline, $n = 6$ mice; *Tie2-tTA;TRE-Notch4** + L-NNA, $n = 6$ mice; $P = 0.0002$, *t* test). (**C**) Fraction of AV connections with a diameter of ≥30 μm over total AV connections quantified [same *n* numbers as in (B); $P < 0.0001$, *t* test]. (**D**) Lectin-perfused vasculature on P12 surface cerebral cortex of *Tie2-tTA* and *Tie2-tTA;TRE-Notch4** mice treated with saline or L-NNA (dashed lines, example AV connections; arrowheads, example points of measurement for AV connection diameter; scale bars, 100 μm). (**E**) AV connection diameter [*Tie2-tTA* + saline, $n = 6$ mice; *Tie2-tTA* + L-NNA, $n = 7$ mice; *Tie2-tTA;TRE-Notch4** + saline, $n = 4$ mice; *Tie2-tTA;TRE-Notch4** + L-NNA, $n = 5$ mice; *Tie2-tTA;TRE-Notch4** + L-NNA versus *Tie2-tTA;TRE-Notch4** + saline, $P_{adj} < 0.0001$; *Tie2-tTA;TRE-Notch4** + L-NNA versus *Tie2-tTA* + saline, $P_{adj} = 0.2631$; *Tie2-tTA;TRE-Notch4** + L-NNA versus *Tie2-tTA* + L-NNA, $P_{adj} = 0.3582$; Tukey's multiple comparisons test following a two-way analysis of variance (ANOVA) to analyze the effects of Notch4*^{EC} and L-NNA]. (**F**) Fraction of AV connections with a diameter of ≥12.5 μm over total AV connections quantified [same *n* numbers as in (E); *Tie2-tTA;TRE-Notch4** + L-NNA versus *Tie2-tTA;TRE-Notch4** + saline, $P_{adj} < 0.0001$; *Tie2-tTA;TRE-Notch4** + L-NNA versus *Tie2-tTA* + saline, $P_{adj} = 0.5605$; *Tie2-tTA;TRE-Notch4** + L-NNA versus *Tie2-tTA* + L-NNA, $P_{adj} = 0.5336$; Tukey's multiple comparisons test following a two-way ANOVA to analyze the effects of Notch4*^{EC} and L-NNA]. Error bars, SEM.

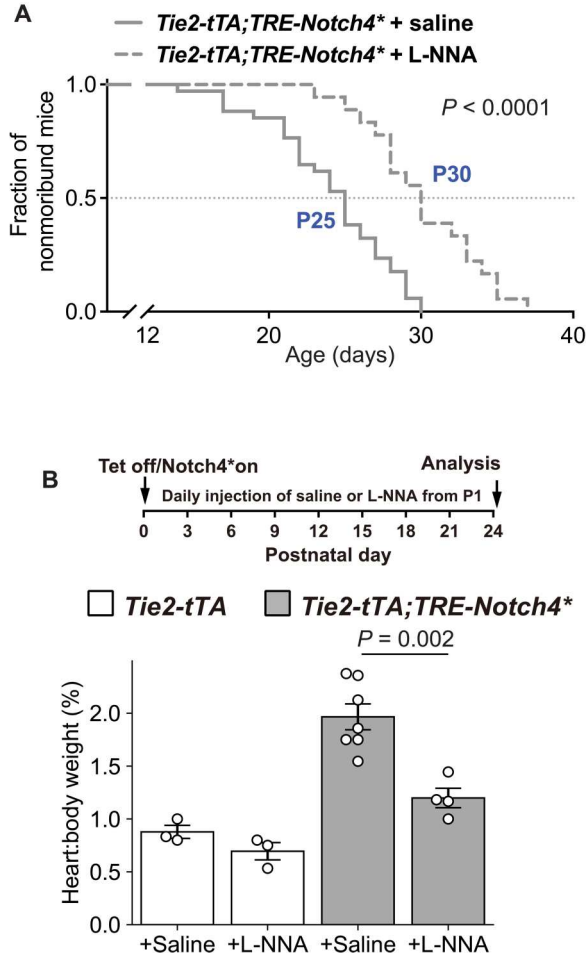

Fig. 4. L-NNA treatment delayed illness progression in mice expressing Notch4* in ECs. (**A**) Kaplan-Meier analysis of *Tie2-tTA;TRE-Notch4** mice treated with saline (n = 34 mice) or L-NNA (n = 18 mice), with monitoring starting on P12. Blue indicates median moribund age (P < 0.0001, log-rank/Mantel-Cox test). (**B**) Heart-to-body weight ratio at P24 (*Tie2-tTA* + saline, n = 3 mice; *Tie2-tTA* + L-NNA, n = 3 mice; *Tie2-tTA;TRE-Notch4** + saline, n = 7 mice; *Tie2-tTA;TRE-Notch4** + L-NNA, n = 4 mice; P = 0.002, t test.). Error bars, SEM.

NOS reduced the overall severity of Notch4^{*EC}-mediated vessel enlargement.

eNOS deletion decreased AVM diameter in brains of mice expressing Notch4* in ECs

To evaluate the effects of deletion of *eNOS* on Notch4^{*EC}-induced brain AVM formation, we examined tomato lectin–perfused whole-mount brain preparations of Notch4^{*EC} mice without and with *eNOS* deletion at P24 (or at moribund if mice became moribund earlier than P24; Fig. 5A and figs. S10 and S11), where Notch4^{*EC} expression was activated at birth by withdrawing tetracycline treatment. Deletion of *eNOS* attenuated Notch4^{*EC}-mediated brain AVM formation at P24. Notch4^{*EC} mice lacking both *eNOS* alleles exhibited decreased AV connection diameter (25 ± 2 versus 34 ± 2 μm with *Tie2-tTA;TRE-Notch4*;eNOS*$^{+/+}$; Fig. 5B) and decreased fraction of severely enlarged AV connections with a diameter of ≥30 μm over total AV connections quantified (27 ± 6 versus 53 ± 4% with *Tie2-tTA;TRE-Notch4*;eNOS*$^{+/+}$; Fig. 5C). Thus, our data suggest that *eNOS* deletion attenuates brain AVM formation in Notch4^{*EC} mice, similar to pan-NOS inhibition by L-NNA treatment, while vessel diameters were variable and individual animals exhibited a wider range of phenotype.

eNOS deletion delayed illness progression in mice expressing Notch4* in ECs

Similar to the treatment of mice with L-NNA, *eNOS* deletion delayed illness in Notch4^{*EC} mice (median moribund age: P28.5 in *Tie2-tTA;TRE-Notch4*;eNOS*$^{-/-}$ mice versus P23 in *Tie2-tTA;TRE-Notch4*;eNOS*$^{+/+}$ mice; Fig. 5D). *eNOS* deletion in genetic controls without Notch4^{*EC} expression did not result in illness or moribundity during this time window. These results suggest that, similar to L-NNA treatment, genetic deletion of *eNOS* delayed disease progression in Notch4^{*EC} mice.

eNOS deletion reduced the severity of cardiomegaly in mice expressing endothelial Notch4*

To assess whether Notch4^{*EC}-associated heart enlargement was affected following *eNOS* deletion, we measured heart-to-body weight ratio at P24. Heart-to-body weight ratio was decreased in *Tie2-tTA;TRE-Notch4*;eNOS*$^{-/-}$ mice compared to *Tie2-tTA;TRE-Notch4*;eNOS*$^{+/+}$ mice (Fig. 5E; images of hearts are shown in fig. S12). These results suggest that similar to L-NNA treatment, *eNOS* deletion reduced the overall severity of Notch4^{*EC}-mediated AV shunting.

Endothelial-specific *eNOS* deletion decreased AVM diameter in brains of mice expressing Notch4* in ECs

eNOS expression is not restricted to ECs. We thus performed postnatal deletion of *eNOS* specifically in ECs using *Tie2-tTA;TRE-Notch4*;Cdh5(PAC)-CreERT2;eNOS*$^{f/f}$ mice, with EC-specific deletion of eNOS verified by whole-mount immunostaining (fig. S13). Endothelial-specific deletion of *eNOS* decreased AV connection diameter at P24 [mean AV connection diameter of 19 ± 2 μm in *Tie2-tTA;TRE-Notch4*;Cdh5(PAC)-CreERT2;eNOS*$^{f/f}$ compared to 35 ± 3 μm in genetic controls; Fig. 5, F and G, and figs. S14 and S15], consistent with Notch4^{*EC} mice with global germline *eNOS* knockout. Similar to *eNOS* global knockout, endothelial-specific *eNOS* deletion delayed illness in Notch4^{*EC} mice [median moribund age: P32 in *Tie2-tTA;TRE-Notch4*;Cdh5(PAC)-CreERT2;eNOS*$^{f/f}$ mice versus P24 in *Tie2-tTA;TRE-Notch4*;eNOS*$^{f/f}$ mice; Fig. 5H]. *eNOS* deletion in genetic controls without Notch4^{*EC} expression did not result in illness or moribundity during this time window. The heart-to-body weight ratio was also decreased in *Tie2-tTA;TRE-Notch4*; Cdh5(PAC)-CreERT2;eNOS*$^{f/f}$ mice compared to *Tie2-tTA;TRE-Notch4*;eNOS*$^{f/f}$ mice (Fig. 5I; images of hearts are shown in fig. S16).

Endothelial Notch4* expression did not result in a significant change in cGMP production in aortae, DAF staining in cerebral vasculature, or nitrite/nitrate levels in isolated cerebral vessels

Our results show that NOS inhibition or *eNOS* deletion attenuated brain AVM initiation and its progression, suggesting a role for eNOS and potentially other NOS isoforms in Notch4^{*EC} mice. We thus investigated whether Notch4^{*EC} expression affected NO production. First, we measured cyclic guanosine monophosphate (cGMP) production, a surrogate for NO production (*25*), in the

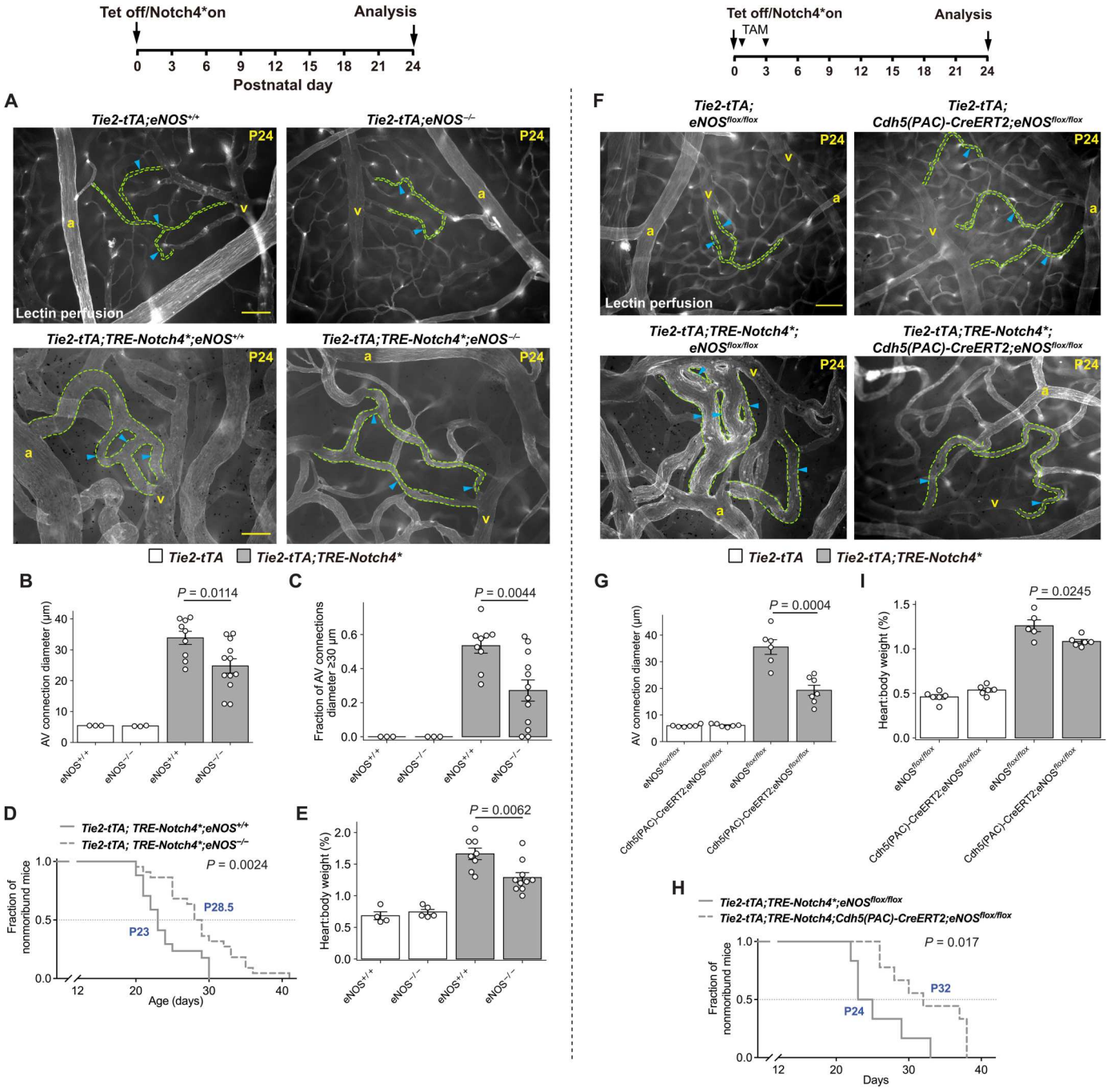

Fig. 5. *eNOS* deletion decreased AVM diameter in brains of mice expressing Notch4* in ECs. (**A**) Vasculature on P24 surface cerebral cortex of *Tie2-tTA* and *Tie2-tTA;TRE-Notch4** mice without ($eNOS^{+/+}$) and with ($eNOS^{-/-}$) endothelial nitric oxide synthase (*eNOS*) deletion. (**B**) AV connection diameter (*Tie2-tTA;TRE-Notch4*;*$eNOS^{+/+}$, $n = 9$ mice; *Tie2-tTA;TRE-Notch4*;*$eNOS^{-/-}$, $n = 12$ mice; $P = 0.0114$, *t* test). (**C**) Fraction of AV connections with a diameter of ≥30 μm over total AV connections quantified [same *n* numbers as in (B); $P = 0.0044$, *t* test]. For (B) and (C), $n = 3$ mice per group for *Tie2-tTA;*$eNOS^{+/+}$ and *Tie2-tTA;*$eNOS^{-/-}$. (**D**) Kaplan-Meier analysis of *Tie2-tTA;TRE-Notch4** mice without ($eNOS^{+/+}$) and with ($eNOS^{-/-}$) *eNOS* deletion (*Tie2-tTA;TRE-Notch4*;*$eNOS^{+/+}$, $n = 17$ mice; *Tie2-tTA;TRE-Notch4*;*$eNOS^{-/-}$, $n = 24$ mice; $P = 0.0024$, log-rank/Mantel-Cox test). (**E**) Heart-to-body weight ratio at P24 (*Tie2-tTA;TRE-Notch4*;*$eNOS^{+/+}$, $n = 8$ mice; *Tie2-tTA;TRE-Notch4*;*$eNOS^{-/-}$, $n = 10$ mice; $P = 0.0062$, *t* test; *Tie2-tTA;*$eNOS^{+/+}$, $n = 4$ mice; *Tie2-tTA;*$eNOS^{-/-}$, $n = 5$ mice). (**F**) Vasculature on P24 surface cerebral cortex of *Tie2-tTA* and *Tie2-tTA;TRE-Notch4** mice without and with endothelial-specific deletion of *eNOS*. (**G**) AV connection diameter [*Tie2-tTA;TRE-Notch4*;*$eNOS^{f/f}$, $n = 6$ mice; *Tie2-tTA;TRE-Notch4*;Cdh5(PAC)-CreERT2;*$eNOS^{f/f}$, $n = 7$ mice; $P = 0.0004$, *t* test; $n = 6$ mice per group for *Tie2-tTA;*$eNOS^{f/f}$ and *Tie2-tTA;Cdh5(PAC)-CreERT2;*$eNOS^{f/f}$]. (**H**) Kaplan-Meier analysis of *Tie2-tTA;TRE-Notch4** mice without and with endothelial-specific *eNOS* deletion [*Tie2-tTA;TRE-Notch4*;*$eNOS^{f/f}$, $n = 6$ mice; *Tie2-tTA;TRE-Notch4*;Cdh5(PAC)-CreERT2;*$eNOS^{f/f}$, $n = 9$ mice; $P = 0.017$, log-rank/Mantel-Cox test]. (**I**) Heart-to-body weight ratio at P24 [*Tie2-tTA;TRE-Notch4*; Cdh5(PAC)-CreERT2;*$eNOS^{f/f}$, $n = 6$ mice; *Tie2-tTA;TRE-Notch4*;*$eNOS^{f/f}$, $n = 5$ mice; $P = 0.0245$, *t* test; *Tie2-tTA;*$eNOS^{f/f}$, $n = 6$ mice; *Tie2-tTA; Cdh5(PAC)-CreERT2;*$eNOS^{f/f}$, $n = 6$ mice]. Dashed lines, example AV connections; arrowheads, example points of measurement for AV connection diameter; scale bars, 100 μm. For Kaplan-Meier analyses, monitoring started on P12, and blue indicates median moribund age. Error bars, SEM.

aortae of Notch4*^{EC} and control mice. We did not detect a change in ACh-stimulated, NO-dependent aortic cGMP production in Notch4*^{EC} mice at P12 (in which Notch4*^{EC} expression was activated at birth) or in adult Notch4*^{EC} mice in which Notch4*^{EC} was expressed for 10 days (these mice are not expected to develop brain AV shunts during this time frame; Fig. 6A) (*10*). These data suggest that Notch4*^{EC} expression did not affect NO production in arteries, either during AVM initiation or independent of brain AVM initiation (in adult mice without brain AVM).

Second, we assessed NO production in cortical sections using the NO indicator 4-amino-5-methylamino-2′,7′-difluorofluorescein (DAF-FM) diacetate. DAF-FM fluorescence was detected in arterial branches but not veins, capillaries, or AV connections in control brains as well as Notch4*^{EC} brains at P12 (Fig. 6B). Mice were treated with L-NNA to measure NOS-dependent NO production. We did not detect differences in L-NNA–sensitive DAF fluorescence between Notch4*^{EC} arterial branches and those of control (Fig. 6C). Third, we assessed nitrite/nitrate level, an indicator of NO production, in isolated brain blood vessels and did not detect a difference between Notch4*^{EC} and control groups at either P12 or P16 (Fig. 6D). Together, the results suggest that Notch4*^{EC} expression did not result in a detectable change in NO in aortae or cerebral vessels.

Tempol treatment delayed illness progression and decreased brain AVM diameter in moribund mice expressing Notch4* in ECs

Our data show that eNOS contributed to AVM formation without statistically significant changes in NO levels. Besides producing NO, eNOS activity may also result in increased generation of cellular oxidants. To test whether increased oxidant levels are involved in Notch4*-mediated brain AVM formation, we used Tempol (4-hydroxy-2,2,6,6-tetramethylpiperidine-1-oxyl), which is a potent, in vivo–compatible antioxidant. Tempol can scavenge biologically relevant free radicals and thus prevent oxidative damage to biomolecules. While Tempol does not directly scavenge hydrogen peroxide, it can inhibit hydrogen peroxide–driven processes and prevent H_2O_2-dependent oxidations by interfering with myeloperoxidase-catalyzed oxidation and nitration processes (*26*, *27*). Notch4*^{EC} expression was activated at birth (P0) by withdrawing tetracycline treatment, and Notch4*^{EC} and genetic control mice were treated with Tempol daily starting on P1. Tempol treatment delayed illness in Notch4*^{EC} mice (median moribund age: P28 + Tempol versus P25 + vehicle; Fig. 7A). Vehicle- or Tempol-treated genetic controls without Notch4*^{EC} did not result in illness or moribundity.

We next evaluated the effects of Tempol on Notch4*^{EC}-mediated brain AVM severity by examining cortical vasculature of severely

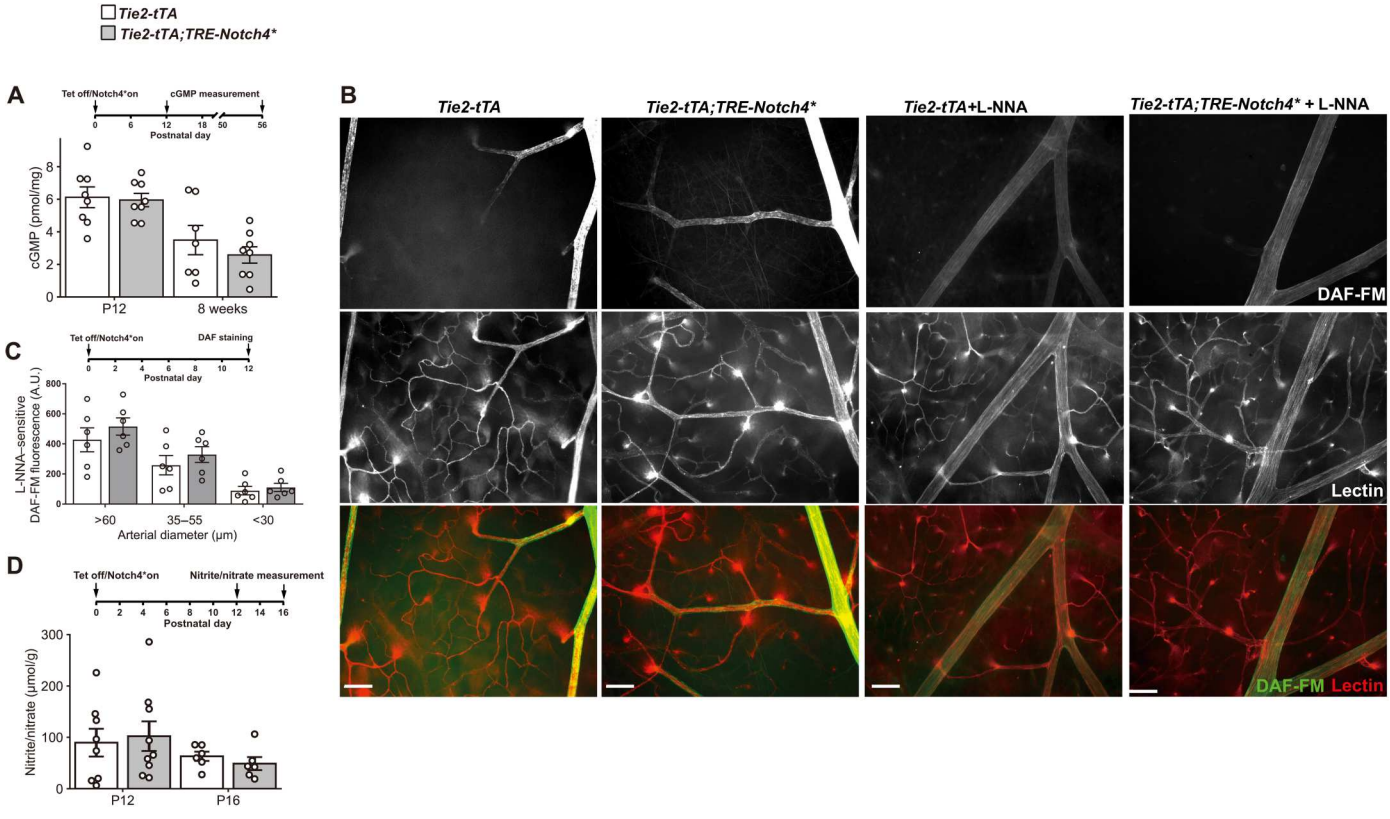

Fig. 6. Endothelial Notch4* expression did not result in a significant change in cGMP production in aortae, DAF staining in cerebral vasculature, or nitrite/nitrate levels in isolated cerebral vessels. (**A**) Acetylcholine (ACh)–stimulated cyclic guanosine monophosphate (cGMP) production in aorta (P12: *Tie2-tTA*, $n = 8$ mice; *Tie2-tTA;TRE-Notch4**, $n = 8$ mice; $P = 0.8248$, *t* test; 8 weeks: *Tie2-tTA*, $n = 7$ mice; *Tie2-tTA;TRE-Notch4**, $n = 8$ mice; $P = 0.3754$, *t* test). (**B**) 4-Amino-5-methylamino-2′,7′-difluorofluorescein (DAF-FM) staining and lectin-perfused vasculature on P12 surface cerebral cortex of *Tie2-tTA* and *Tie2-tTA;TRE-Notch4**, with or without L-NNA treatment. Scale bars, 100 μm. (**C**) Quantification of L-NNA sensitive DAF-FM fluorescence intensity by arterial diameter (A.U., arbitrary units; *Tie2-tTA*, $n = 6$ mice; *Tie2-tTA;TRE-Notch4**, $n = 6$ mice; > 60 μm, $P = 0.389$; 35 to 55 μm, $P = 0.4138$; <30 μm, $P = 0.5951$, *t* test.) (**D**) Nitrite/nitrate level in isolated brain blood vessels at P12 (*Tie2-tTA*, $n = 8$ mice; *Tie2-tA;TRE-Notch4**, $n = 9$ mice; $P = 0.7562$, *t* test) and P16 ($n = 6$ for both groups; $P = 0.3785$, *t* test). Error bars, SEM.

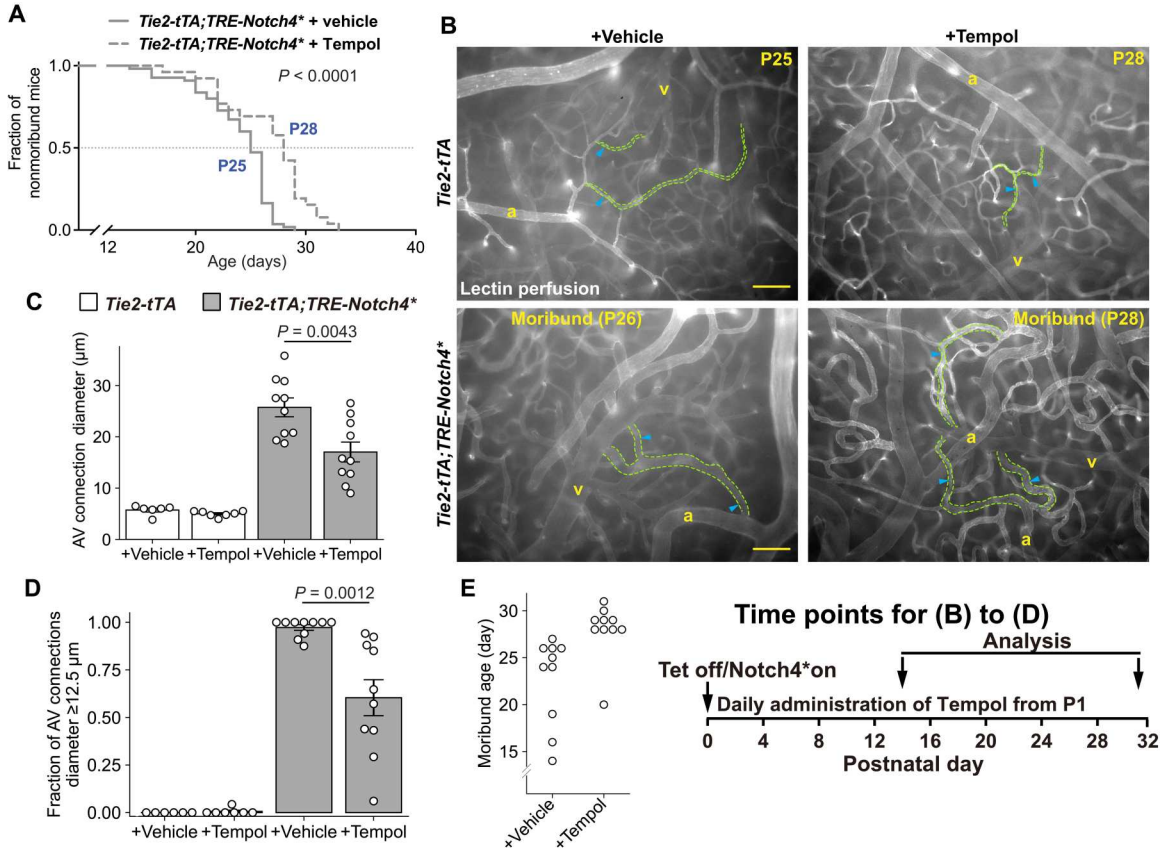

Fig. 7. Tempol treatment delayed illness progression and decreased brain AVM diameter in moribund mice expressing Notch4* in ECs. (**A**) Kaplan-Meier analysis of *Tie2-tTA;TRE-Notch4** mice treated with vehicle ($n = 55$ mice) or Tempol (4-hydroxy-2,2,6,6-tetramethylpiperidine-1-oxyl; $n = 26$ mice), with monitoring starting on P12. Blue indicates median moribund age ($P < 0.0001$, log-rank/Mantel-Cox test). (**B**) Lectin-perfused vasculature on surface cerebral cortex of moribund *Tie2-tTA;TRE-Notch4** mice and age-matched *Tie2-tTA* mice treated with vehicle or Tempol (dashed lines, example AV connections; arrowheads, example points of measurement for AV connection diameter; scale bars, 100 μm). (**C**) AV connection diameter (*Tie2-tTA* + vehicle, $n = 6$ mice; *Tie2-tTA* + Tempol, $n = 7$ mice; *Tie2-tTA;TRE-Notch4** + vehicle, $n = 10$ mice; *Tie2-tTA;TRE-Notch4** + Tempol, $n = 10$ mice; $P = 0.0043$, *t* test). (**D**) Fraction of AV connections with a diameter of ≥12.5 μm over total AV connections quantified [same *n* numbers as in (C); $P = 0.0012$, *t* test]. (**E**) Age at which *Tie2-tTA;TRE-Notch4** mice were moribund. Error bars, SEM.

affected, moribund Notch4^{*EC} mice. At moribund, Tempol-treated Notch4^{*EC} mice exhibited less severe AVM compared to vehicle-treated Notch4^{*EC} mice (Fig. 7B and fig. S17), with decreased AV connection diameter (17 ± 2 μm + Tempol versus 26 ± 2 μm + vehicle) and smaller fraction of enlarged AV connections with a diameter of ≥12.5 μm over total AV connections quantified (60 ± 9% + Tempol versus 97 ± 1% + vehicle), despite being harvested at older ages (Fig. 7, C to E). Tempol- or vehicle-treated genetic controls without Notch4^{*EC} expression exhibited no gross vascular phenotype. Together, these data show that Tempol attenuated Notch4^{*EC}-mediated brain AVM formation and delayed brain AVM-associated moribundity. However, when Tempol was administered from P16 with established AVMs, AV connection diameter in Tempol-treated Notch4^{*EC} mice (29 ± 4 μm) was not statistically different from that in saline-treated Notch4^{*EC} mice (34 ± 2 μm; fig. S8), suggesting that Tempol treatment was insufficient to reverse established AVMs.

Increased hydrogen peroxide, but not superoxide or peroxynitrite levels detectable in isolated cerebral vessels of mice expressing Notch4* in ECs

Because one of the best-known protective effects of Tempol is its action as a superoxide dismutase (SOD) mimetic (*28*), we measured superoxide radical anion production in isolated brain vessels, using a liquid chromatography–mass spectrometry (LC-MS) assay that used hydroethidine (HE) as a probe. We monitored the superoxide-specific product 2-hydroxyethidium (2-OH-E$^+$; formed from the reaction between HE and superoxide radical anion). However, we did not detect a statistically significant increase in either total SOD-sensitive or L-NG-nitro arginine-methyl ester (L-NAME)–sensitive 2-OH-E$^+$ levels between Notch4^{*EC} and control brain vessels (fig. S18).

To further assess the potential formation of cellular oxidants that can lead to vascular dilation, we used the state-of-the-art mass spectrometric boronate probe, *o*-MitoPhB(OH)$_2$, and measured its oxidation and nitration products in isolated brain blood vessels of Notch4^{*EC} and control mice. The level of the major oxidation product, *o*-MitoPhOH, was higher in Notch4^{*EC} brain blood vessels compared to that of controls and was reduced by L-

NAME treatment (Fig. 8A). We further used the *o*-MitoPhB(OH)$_2$ probe to discriminate between H_2O_2- and $ONOO^-$-mediated oxidation (*29*). LC–tandem MS analyses showed increased levels of the phenolic product, *o*-MitoPhOH, but not $ONOO^-$-specific product, cyclo-o-MitoPh. As expected, treatment of the vessel with the peroxynitrite generator, SIN-1, led to the appearance of the cyclo-o-MitoPh product (Fig. 8B). These data suggest a NOS-dependent increase in hydrogen peroxide but not peroxynitrite production in brain vessels of mice expressing Notch4*^{EC}. Last, because H_2O_2 can lead to 3-nitrotyrosine (3-NT) production upon peroxidase-catalyzed oxidation of nitrite (*30*–*32*), we performed immunofluorescence staining of 3-NT and showed increased protein tyrosine nitration in the cortex of Notch4*^{EC} mice, with higher 3-NT levels in Notch4*^{EC} arteries, veins, and capillaries compared to that of controls (Fig. 8, C and D).

DISCUSSION

Here, we report several findings on the molecular mechanism underlying AVM formation (fig. S19). First, the expression of activated

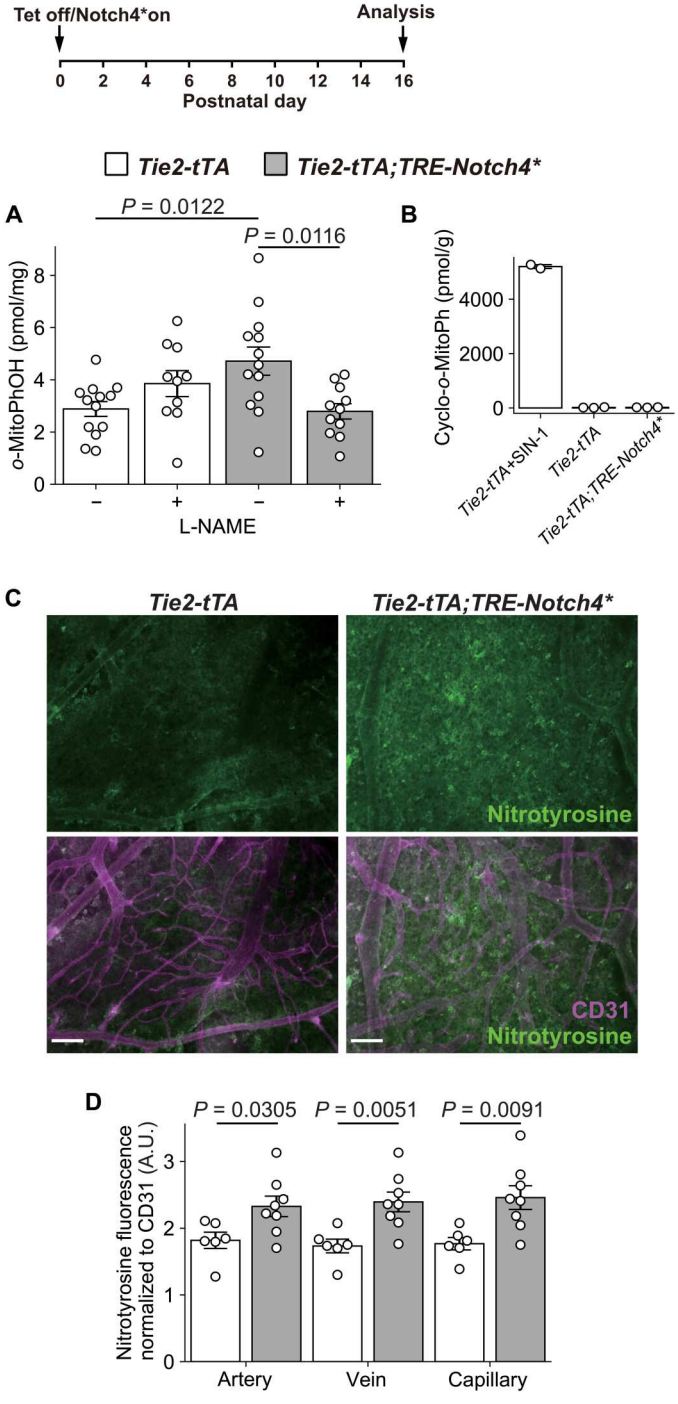

Fig. 8. Increased hydroperoxide and NT but not peroxynitrite levels in isolated cerebral vessels of mice expressing Notch4* in ECs. (**A**) Hydrogen peroxide product *o*-MitoPhOH in isolated brain blood vessels at P16 [*Tie2-tTA* + vehicle, $n = 13$ mice; *Tie2-tTA* + NG-nitro arginine-methyl ester (L-NAME), $n = 10$ mice; *Tie2-tA;TRE-Notch4** + vehicle, $n = 13$ mice; *Tie2-tA;TRE-Notch4** + L-NAME, $n = 11$ mice; *Tie2-tTA* + vehicle versus *Tie2-tTA;TRE-Notch4** + vehicle, $P_{adj} = 0.0122$; *Tie2-tTA* + vehicle versus *Tie2-tTA* + L-NAME, $P_{adj} = 0.3899$; *Tie2-tTA;TRE-Notch4** + vehicle versus *Tie2-tTA;TRE-Notch4** + L-NAME, $P_{adj} = 0.0116$; Tukey's multiple comparisons test following a two-way ANOVA to analyze the effects of Notch4*^{EC} and L-NAME]. (**B**) Peroxynitrite-specific product cyclo-*o*-MitoPh in isolated brain blood vessels at P16. Cyclo-*o*-MitoPh was below the detection limit for *Tie2-tTA* and *Tie2-tTA;TRE-Notch4** blood vessels. *Tie2-tTA* blood vessels treated with SIN-1 served as a positive control for peroxynitrite. (**C**) Expression of 3-nitrotyrosine (3-NT) in brain blood vessels at P16. Scale bars, 100 μm. (**D**) Fluorescence intensity of 3-NT normalized to that of CD31 (*Tie2-tTA*, $n = 6$ mice; *Tie2-tA;TRE-Notch4**, $n = 8$ mice; artery, $P = 0.0305$; vein, $P = 0.0051$; capillary, $P = 0.0091$, *t* test). Error bars, SEM.

Notch4* in ECs compromises vascular tone, which contributes to the hyperdilation of capillaries, enlargement of AV connections, and AVM initiation. Second, eNOS is involved in Notch4^{*EC}-mediated AVM formation. Third, Notch4^{*EC} increases eNOS-dependent hydrogen peroxide production and protein tyrosine nitration, which can compromise vascular tone and contribute to AVM formation. This study may open future investigations to further elucidate mechanisms underlying AVM pathogenesis as well as Notch regulation of vascular pathophysiology.

We have reported that Notch4* expression in the endothelium disrupted biological control of blood flow by allowing the selective growth of higher-flow/lower-resistance AV connections, at the expense of lower-flow/higher-resistance AV connections, while the nearby lower-flow AV connections regress (*13*). This work led us to the hypothesis of the current paper that vascular tone is compromised in the Notch4* mice, thereby permitting and perpetuating higher-flow AV shunt growth into larger, focal AVMs. Supporting this hypothesis, ex vivo data in isolated mesenteric arteries from HHT type 1 heterozygous knockout mice (*33*) and computational modeling (*34*) suggest that compromised vascular tone contributes to HHT pathology. In addition, mice lacking serum response factor in smooth muscle cells lose contractile protein expression and develop retinal AV shunts (*35*). However, direct measurement of impaired arterial tone in animals that develop AVMs has been lacking. We demonstrate here that vessels connected to AVMs exhibited compromised vascular tone in vivo. Arteriolar tone was compromised in Notch4^{*EC} brains during the early stage of AVM formation, suggesting that decreased vascular tone may be a causal mechanism in AVM formation. Additional support for this notion comes from our ex vivo arterial tone data, where the arterial tone was reduced in isolated arteries from asymptomatic Notch4^{*EC} mice. The ex vivo study in asymptomatic mice is advantageous in revealing the primary effect of Notch4^{*EC} on arterial tone without confounding factors from the complex in vivo environment. Last, inhibiting NOS abolished Notch4*-mediated arterial tone impairment both in vivo and ex vivo and attenuated AVM formation.

While the reduced vascular tone is critical for AVM formation in immature Notch4^{*EC} mice, the reduced arterial tone detected in adult Notch4^{*EC} asymptomatic mice was insufficient to induce brain AVMs within 10 days of Notch4^{*EC} expression induction. We believe that the reduced arterial tone in the adult Notch4^{*EC} brain was not sufficiently severe to induce brain AVMs. There may be other temporal factors required for brain AVM formation. Our data, however, suggest that impaired cerebral vascular tone contributes to brain AVM formation. Furthermore, our data suggest that reduced vascular tone in the upstream arteriolar system results in capillary enlargement (i.e., enlargement of AV shunts), initiating AVMs in immature brains.

The conclusion that reduced vascular tone leads to capillary enlargement is also supported by our data showing that about 40% of ECs in the enlarging capillaries do not express Notch4*. These Notch4*-negative ECs were part of enlarged AV shunts due to compromised vascular tone. We did not notice regional expression of Notch4* that was correlated to AVM formation; instead, the positive and negative Notch4*-expressing cells were evenly distributed throughout the vasculature. Compromised vascular tone, particularly arteriolar tone, led to both capillary enlargements and subsequent flow-perpetuated focal AVM growth. This mosaic and even distribution of Notch4*-positive cells suggest that a mosaic expression pattern is sufficient to induce AVM formation in this animal model. This finding is relevant, as somatic mutations (likely mosaic) are found in humans (*8*). Therefore, uniform expression of causal gene is not required; rather, mosaic expression is sufficient to compromise vascular tone leading to AVM formation.

Inhibition of NOS by L-NNA, which restored arterial tone, attenuated AVMs in immature Notch4^{*EC} mice. It is currently unclear, however, whether Notch4^{*EC} acts directly on the upstream arteriolar system, capillaries, or both, as changes in capillaries can send retrograde signals to regulate vascular tone of the upstream arterial system (*36*). Regardless, our data suggest that reduced arteriolar tone contributes to AVM formation.

The presented data also suggest that eNOS modulates Notch4^{*EC}-mediated vascular tone defects and brain AVM formation. Notch4^{*EC} increased eNOS-mediated hydrogen peroxide production. Hydrogen peroxide can compromise vascular tone, potentially initiating AVMs. Our data also show that NOS inhibitor L-NNA attenuated AVM initiation in Notch4^{*EC} mice. Furthermore, both postnatal endothelial deletion and global germline deletion of eNOS attenuated AVM formation in Notch4^{*EC} mice. Although eNOS deletion results in an impaired vascular tone in mice (*37*), it did not lead to detectable changes in AV diameter connections in eNOS-deficient mice in the absence of Notch4* (Fig. 5, B and G). Together, these results suggest that eNOS signaling contributes to Notch4^{*EC}-mediated brain AVM formation.

Beyond eNOS, another NOS in ECs, neuronal NOS (nNOS), may also contribute to Notch4^{*EC}-mediated brain AVM formation. Increased nNOS levels are known to functionally compensate for eNOS deficiency (*38*–*40*). Supporting this notion, pharmacological inhibition of NOS attenuated Notch4^{*EC}-mediated brain AVM formation more robustly than eNOS genetic deletion. Together, these data suggest that NOS signaling modulates Notch4^{*EC}-mediated brain AVM formation.

Our results also suggest that NOS-dependent production of hydrogen peroxide is involved in the regulation of vascular tone in the Notch4^{*EC} brain AVM mouse model. We detected increased and L-NAME–sensitive hydrogen peroxide production in Notch4^{*EC} brain vessels. Increased protein nitration in Notch4^{*EC} brain vessels without the formation of peroxynitrite suggests that hydrogen peroxide drives protein nitration in the presence of nitrite and myeloperoxidase (*30*, *31*). Furthermore, our functional data show that either inhibition of eNOS/NOS or the presence of Tempol antioxidant (*41*) attenuated AVM formation. Hydrogen peroxide is known to cause vasodilation (*42*, *43*). Together, our data support a model in which increased eNOS-mediated hydrogen peroxide and reduced vascular tone contribute to Notch4^{*EC}-mediated AVM formation.

While hydrogen peroxide levels and protein nitration were higher in Notch4^{*EC} brain vessels, we did not detect statistically significant changes in levels of NO or nitrite/nitrate in Notch4^{*EC} brain vessels or in cGMP levels in Notch4^{*EC} aortae. Overexpression of a gain-of-function Notch mutant in cultured human umbilical vein ECs (HUVECs) increases eNOS activity and NO levels (*44*). It is possible that these HUVECs contain pure ECs and thus exhibit higher NO levels than our isolated brain vessels with a small fraction of ECs, 40% of which were negative for Notch4*. It is also possible that these HUVECs overexpress higher levels of gain-of-function Notch mutations in vitro and thus more robustly promote NO detection than Notch4^{*EC} in brain vessels in vivo.

Even if Notch gain-of-function mutations, including Notch4*, increase NO production, it would be consistent with the reduced vascular tone and AVM formation seen in our Notch4^{*EC} mice. Therefore, it is possible that Notch4^{*EC} affected eNOS, which, in turn, reduces Notch4^{*EC}-mediated vascular tone and thus may further promote AVM formation.

Somatic activating mutations in *KRAS* (*KRASG12V*) were recently identified, with high prevalence in brain AVM patient samples (*8*, *35*). The link between KRAS and Notch is currently under investigation. Expression of KRAS^{G12V} in HUVECs up-regulates Notch pathway genes, e.g., *DLL4*, *JAG1*, *JAG2*, *NOTCH1*, *HES1*, and *HEY2* (*8*, *45*). In another study, expression of KRAS^{G12D} also up-regulates Notch2, Notch4, hairy/enhancer-of-split related with YRPW motif 1 (HEY1), and HEY2 in HUVECs (*45*, *46*). However, there were no detectable changes in the expression of Notch ligand Dll4 in zebrafish expressing KRAS^{G12D} in the endothelium (*47*). Therefore, continued studies are needed to ascertain the link between KRAS and Notch signaling.

MATERIALS AND METHODS

Mice

Tie2-tTA and *TRE-Notch4** mice were generated as previously described (*10*, *48*). *eNOS*$^{-/-}$ (*NOS3*$^{-/-}$) (*49*), *eNOS*$^{f/f}$ (*50*), and *Cdh5(PAC)-CreERT2* (*51*) lines have been published. The genetic background of the mice used in this study was FVB/N or 3+ generations backcrossed into FVB/N background with eNOS knockout. Both male and female mice were used for experiments, except that male mice were used for measuring arterial tone ex vivo. *Tie2-tTA*, which expresses tetracycline-controlled transactivator (tTA), was used as our baseline control; the *Tie2-tTA* control mice do not develop any AVM phenotype. Notch4* expression was regulated in *Tie2-tTA;TRE-Notch4** mice as previously described (*14*). Tetracycline solution [tetracycline (0.5 mg/ml) and sucrose (50 mg/ml); Sigma-Aldrich] was administered to pregnant mothers from mating or plugging and withdrawn from pups at birth. L-NNA (30 mg/kg in saline; Sigma-Aldrich) was administered intraperitoneally (intragastrically before P11). Tempol (50 mg/kg in saline; Sigma-Aldrich) was administered intraperitoneally (intragastrically before P11) and was additionally supplied in drinking water (5 mg/ml). Animals were maintained and treated in accordance with the guidelines of the University of California San Francisco Institutional Animal Care and Use Committee with approved protocol number: AN199765-00.

Arterial tone, arteriolar tone, and ACh-induced vasodilation in vivo

For in vivo intravital imaging at P16, endothelial Notch4* expression was induced at birth by withdrawing tetracycline treatment. Mice were anesthetized with combined 17.5% ketamine (100 mg/ml; Zoetis) and 2.5% xylazine (100 mg/ml; Akorn Animal Health) diluted in physiological saline (Henry Schein Animal Health) and intraperitoneally administered 0.01 ml/g mouse weight. After surgical plane anesthesia was achieved, surgery proceeded as described previously (*24*). Briefly, a steel plate with a diameter of ~2 mm was attached to the parietal skull using a 1:1 ratio of dental cement and cyanoacrylate glue. The head plate was then secured to the holding frame, and a circular craniectomy was performed. After dura opening, first aCSF and then aCSF lacking calcium but containing 1 μM L-type Ca^{2+} channel inhibitor nifedipine (called "Ca^{2+}-free aCSF + nifedipine" thereafter) were pipetted onto the exposed surface of the brain. For L-NNA–treated groups, L-NNA (30 mg/kg) was injected 15 min before image capture followed by Ca^{2+}-free aCSF + nifedipine pipetted onto the exposed surface of the brain. Images were acquired using a stereo microscope (Leica MZ12.5) with an attached camera (Zeiss AxioCam ICc5). Pial arteries (diameter range in aCSF: 20 to 67 μm) and their first-order arterioles (12 to 38 μm) were identified and analyzed using ImageJ [National Institutes of Health (NIH)]. Images were analyzed under a magnification of ×200 to clearly show the boundary of the arterioles. Two locations in the arteries and two locations in the arterioles were analyzed per mouse for the majority of the experiments. The diameters of arteries/arterioles in each mouse were quantified by two experimenters blindly, and results for the vascular tone of arteries or arterioles in each mouse were averaged for comparison. Statistically significant differences between mutant and control groups were additionally analyzed by performing edge detection on intensity line profiles at locations determined by one to two blind experimenters (further described below). Arterial and arteriolar tone were expressed as a decrease in diameter relative to the diameter obtained when incubated in Ca^{2+}-free aCSF + nifedipine (1 μM): $[(D2 - D1)/D2 \times 100\%$, where $D2$ = diameter in Ca^{2+}-free aCSF + nifedipine and $D1$ = diameter in aCSF]. Arterial and arteriolar tone with L-NNA treatment was calculated as: $[(D2 - D1)/D2 \times 100\%$, where $D2$ is diameter in Ca^{2+}-free aCSF + nifedipine and $D1$ is diameter in aCSF + L-NNA injection]. ACh-induced vasodilation was expressed as the percentage change in diameter before and after ACh treatment: $[(D2 - D1)/D1 \times 100\%$, where $D2$ is diameter after ACh treatment and $D1$ is diameter before ACh treatment].

Vessel diameter estimate from intensity line profiles

Rectangular selections (representing vessel segments of interest) of shape $m \times n$, consisting of m intensity line profiles perpendicular to the vessel wall and spanning the vessel boundaries (where $n >$ is the apparent vessel segment diameter), were acquired at the approximate same locations as those used for manual measurements. Edge detection was performed on individual line profiles by convolving the line profile with the one-dimensional Laplace filter [1, −2, 1] and finding the zero-crossings. Zero-crossings with the largest positive and largest negative local intensity variation (window length of three pixels) were identified as the two edges for computing vessel diameter. The diameter of the vessel segment of interest was estimated from the trimmed mean (discarding the lowest 10% and the highest 10%) of m diameters.

Arterial tone measurements ex vivo

Male mice were used at 5 to 6 weeks old. Notch4^{*EC} expression was repressed from birth until 10 days before tissue harvest when tetracycline was withdrawn. Posterior cerebral arteries with diameters on the order of 100 μm were isolated and cannulated on glass micropipettes in a 5-ml myograph chamber (Living Systems Instrumentation), as previously described (*52*, *53*). Arteries were pressurized to 20 mmHg and allowed to equilibrate while continuously superfused (37°C, 30 min, 3 to 5 ml/min) with physiological saline solution (PSS) consisting of: 119 mM NaCl, 4.7 mM KCl, 2 mM $CaCl_2$, 24 mM $NaHCO_3$, 1.2 mM KH_2PO_4, 1.2 mM $MgSO_4$, 0.023 mM EDTA, and 10 mM D-glucose aerated with 5% CO_2/20% O_2

(balance N_2). Bath pH was closely monitored and maintained at 7.35 to 7.40. Following equilibration, contractile function was confirmed in arteries upon challenge with 60 mM $[K^+]_o$, made by isosmotic replacement of NaCl with KCl. After washout (10 min), intravascular pressure was increased to 40, 60, 80, and 100 mmHg. In a set of experiments, intravascular pressure was increased to 60 mmHg before application of L-NNA (50 μM). The luminal diameter of arteries was continuously recorded with a charge-coupled device camera and the edge detection function of IonOptix software. Arterial tone was expressed as a decrease in diameter relative to the maximum passive diameter at a given intravascular pressure obtained at the end of each experiment using Ca^{2+}-free PSS containing the L-type Ca^{2+} channel inhibitor nifedipine (1 μM): [(DP − DA)/DP × 100%, where DP is passive (in 0 Ca^{2+}/nifedipine PSS solution) diameter and DA is active (in Ca^{2+} containing PSS solution) diameter].

Fluorescent probes, immunostaining, and imaging

For lectin perfusion, fluorescence-conjugated *Lycopersicon esculentum* lectin (Vector Laboratories) was injected into the inferior vena cava as previously described (*10*, *14*). VE-cadherin staining [BD Pharmingen, 555289, clone 11D4.1, Research Resource Identifier (RRID):AB_395707] and Notch4ICD staining (Millipore, 07-189, RRID:AB_11211117) were performed as previously described (*54*). For 3-NT staining, mice were transcardially perfused with saline, followed by 4% paraformaldehyde (PFA). Cortex slices were dissected and postfixed overnight in 4% PFA. Cortex slices were then blocked in tris-buffered saline (TBS) containing 3% donkey serum and 0.2% Triton X-100 for 1 hour at room temperature, followed by incubation with mouse monoclonal anti-NT antibody (39B6) (1:100; Santa Cruz Biotechnology, sc-32757, RRID:AB_628022) overnight at 4°C. After three washes with TBST (TBS containing 0.1% Triton X-100), samples were incubated with donkey anti-mouse Alexa Fluor 488 (1:1000; Molecular Probes, A-21202, RRID:AB_141607) overnight in 4°C. After three washes with TBST, samples were imaged. For eNOS staining, mice were transcardially perfused with 1% PFA. Cortex slices were dissected and postfixed for 2 hours in 4% PFA. After washing with phosphate-buffered saline (PBS), samples were blocked in PBS with 3% donkey serum, 0.2% Triton X-100, and 2% bovine serum albumin (BSA) overnight and then incubated with anti-eNOS antibody (1:100; Thermo Fisher Scientific, PA1-037, RRID:AB_325774) overnight. After three washes with PBS containing 0.1% Triton X-100, samples were incubated with donkey anti-rabbit Alexa Fluor 488 (1:1000; Molecular Probes, A-21206, RRID:AB_2535792) for 2 hours at room temperature. eNOS fluorescence intensity was calculated as the intensity of the vascular area minus the intensity of the nonvascular area. Imaging was performed using an Axioskop 2 Plus microscope (Zeiss) and SlideBook software (Intelligent Imaging Innovations).

Measurement of AV connection diameter

AV connection diameters were measured at their narrowest point as previously described (*13*). To compute the mean AV connection diameter for each animal, AV connections were quantified from 5+ fields of view of ~900 by 700 μm^2 using ImageJ. We additionally computed the fraction of AV connections with a diameter of ≥12.5 μm over total AV connections quantified (indicating enlarged AV connections) or ≥30 μm (indicating severely enlarged AV connections).

Moribundity

Moribundity was assessed using criteria from the NIH Office of Animal Care and Use guidelines (https://oacu.oir.nih.gov/). The moribund condition is defined as a clinically irreversible condition leading inevitably to death. Commonly used signs of moribundity include but are not limited to: (i) lack of responsiveness to manual stimulation, (ii) immobility, (iii) an inability to eat or drink. Moribundity was assessed in an unbiased manner during a daily routine health check by trained veterinary nurses who were unaware of the experimental information. The vet nurses inform researchers when the mice have reached a moribund state.

cGMP assay

Tissue cGMP levels were measured as previously described (*55*). Briefly, 2-mm aortic segments were incubated in Dulbecco's modified Eagle's medium containing antibiotics for 3 hours and then with or without NOS inhibitor L-NNA (2 mM) for 30 min. Aortic segments were preincubated with phosphodiesterase inhibitor 3-isobutyl-1-methylxanthine (IBMX; 200 μM) for 5 min and stimulated with ACh (2 μM) for 5 min in the presence of IBMX. Because of the size of P12 aortae, basal (non–ACh-stimulated) cGMP production was not measured. Tissues were snap-frozen in liquid nitrogen and homogenized. cGMP levels were assayed using cGMP Enzyme Immunoassay Biotrak System, Amersham RPN 226 (GE Healthcare) according to the manufacturer's instructions. NOS-dependent cGMP production was calculated by subtracting the value in the presence of L-NNA.

Blood vessel isolation

Blood vessels were isolated from the brain by Dextran centrifugation (*56*). Briefly, the brain was removed and cut into six pieces in cold (4°C) modified Krebs-Ringer bicarbonate solution (NaCl, 118.6 mmol/liter; KCl, 4.7 mmol/liter; CaCl2, 2.5 mmol/liter; MgSO4, 1.2 mmol/liter; KH2PO4, 1.2 mmol/liter; NaHCO3, 25.1 mmol/liter; glucose, 10.1 mmol/liter; and EDTA, 0.026 mmol/liter). The brain was then homogenized in ice-cold PBS with a Dounce homogenizer and centrifuged at 2000*g* at 4°C. The supernatant was discarded, and the pellet was suspended and layered over 15% Dextran (Sigma-Aldrich) in PBS and centrifuged at 3200*g* for 45 min at 4°C. The vessel pellet was resuspended in 1% BSA and was then passed through a 40-μm cell strainer (BD Falcon). Vessels retained on the mesh were washed with 1% BSA/PBS and collected by centrifugation at 3000*g* for 10 min at 4°C.

Measurement of NO

For DAF-FM staining, whole-mount cortical sections were incubated in Krebs-Hepes buffer with 20 μM freshly diluted DAF-FM diacetate (Invitrogen, D23844) for 60 min at room temperature. Samples were washed twice with PBS and washed in 0.1% Triton X-100 in PBS for 10 min before imaging. L-NNA (30 mg/kg in saline; Sigma-Aldrich) was administered intraperitoneally 48 and 24 hours before harvest and added during incubation at 1 mg/ml concentration. DAF-FM fluorescence intensity was quantified using ImageJ in three types of vessel segments grouped by their diameter: >60 (large), 35 to 55 (medium), and <30 μm (small). We left a 5-μm gap between the diameter bins to ensure clear separation

between them. The L-NNA–sensitive intensity was calculated by subtracting values from L-NNA–treated samples for the same segment. Total nitrite and nitrate (NO_3 + NO_2) were measured using a commercially available fluorometric nitrite/nitrate assay kit according to the manufacturer's instructions (Cayman Chemical). The assay is based on nitrite-mediated nitrosation of 2,3-diaminonaphthalene to a fluorescent triazole derivative under acidic conditions. Nitrate anion is reduced to nitrite with the help of nitrate reductase before nitrite measurements.

Measurement of superoxide radical anion

Superoxide radical anion ($O_2^{\bullet-}$) levels in brain blood vessels were measured by LC-MS–based detection of 2-OH-E^+, which is the specific product of the reaction of $O_2^{\bullet-}$ with hydroethidine (HE; also known as dihydroethidium) (Invitrogen). Briefly, freshly isolated blood vessels from one mouse were equally divided into three parts and pretreated with saline, 50 μM L-NAME (Sigma-Aldrich), or SOD–polyethylene glycol (100 U/ml) (Sigma-Aldrich, S9549) in Krebs-Hepes buffer for 30 min. HE was then added to blood vessels to a final concentration of 50 μM in the buffer and incubated at 37°C for 30 min. After rinsing with ice-cold buffer, the vessels were centrifuged, collected, and kept at −80°C until analyses. Immediately before analyses, HE and its oxidation products were extracted from the vessels with ice-cold acetonitrile (50 μl/mg tissue) containing 0.1% formic acid and 3,8-diamino-6-phenylphenanthridine as an internal standard. After 30 min of shaking at 4°C, the samples were centrifuged (30 min × 20,000*g* at 4°C), and the supernatant (1 vol) was diluted with water containing 0.1% formic acid (3 vol). After additional centrifugation (15 min × 20,000*g* at 4°C), the supernatants were transferred into high-performance LC (HPLC) vials and analyzed by LC-MS, according to a published protocol (*57*, *58*).

Measurement of hydrogen peroxide and peroxynitrite

Hydrogen peroxide (H_2O_2) and peroxynitrite ($ONOO^-$) levels in brain blood vessels were measured by LC-MS–based profiling of their products generated in reaction with a triphenylphosphonium-linked phenylboronic acid probe, *o*-MitoPhB$(OH)_2$ (*29*, *59*, *60*). Briefly, freshly isolated blood vessels from two mice were pooled together and incubated in modified Krebs-Ringer bicarbonate solution for 15 min with or without 50 μM L-NAME treatment. Then, *o*-MitoPhB$(OH)_2$ was added to blood vessels to a final concentration of 50 μM and incubated at 37°C for 90 min. After rinsing with ice-cold buffer, the vessels were centrifuged, collected, and stored at −80°C until LC-MS analyses. Immediately before analyses, *o*-MitoPhB$(OH)_2$ and its oxidation and nitration products were extracted from the vessels with ice-cold acetonitrile (10 μl/mg tissue) containing 0.1% formic acid and (2-methylbenzyl) triphenylphosphonium chloride (*o*-MitoPhCH_3) as an internal standard. After 30 min of shaking at 4°C, the samples were centrifuged (30 min × 20,000*g* at 4°C), and the supernatant (1 vol) was diluted with water containing 0.1% formic acid (3 vol). After additional centrifugation (15 min × 20,000*g* at 4°C), the supernatants were transferred into HPLC vials and analyzed by LC-MS, as described previously (*29*). The phenolic product (*o*-MitoPhOH) served as a general oxidation product common for H_2O_2 and $ONOO^-$, while cyclo-*o*-MitoPh and *o*-Mito$PhNO_2$ served as specific products of $ONOO^-$ (*29*). Samples treated with 100 μM SIN-1 served as a positive control for $ONOO^-$ detection.

Statistical analysis

Results are presented as means ± SEM unless otherwise specified. Two-tailed, unpaired Student's *t* test was used to compare means between two groups unless otherwise specified. Statistical analysis was performed using Prism (GraphPad), and $P < 0.05$ was considered statistically significant. The numbers of biological replicates are indicated in the figure legends.

Supplementary Materials

This PDF file includes:

Figs. S1 to S19

View/request a protocol for this paper from *Bio-protocol*.

REFERENCES AND NOTES

1. R. M. Friedlander, Arteriovenous malformations of the brain. *N. Engl. J. Med.* **356**, 2704–2712 (2007).
2. M. T. Lawton, W. C. Rutledge, H. Kim, C. Stapf, K. J. Whitehead, D. Y. Li, T. Krings, K. terBrugge, D. Kondziolka, M. K. Morgan, K. Moon, R. F. Spetzler, Brain arteriovenous malformations. *Nat. Rev. Dis. Primers.* **1**, 15008 (2015).
3. P. A. Murphy, G. Lu, S. Shiah, A. W. Bollen, R. A. Wang, Endothelial Notch signaling is upregulated in human brain arteriovenous malformations and a mouse model of the disease. *Lab. Investig.* **89**, 971–982 (2009).
4. Q. ZhuGe, Z. Wu, L. Huang, B. Zhao, M. Zhong, W. Zheng, C. GouRong, X. Mao, L. Xie, X. Wang, K. Jin, Notch4 is activated in endothelial and smooth muscle cells in human brain arteriovenous malformations. *J. Cell. Mol. Med.* **17**, 1458–1464 (2013).
5. Q. ZhuGe, M. Zhong, W. Zheng, G. Y. Yang, X. Mao, L. Xie, G. Chen, Y. Chen, M. T. Lawton, W. L. Young, D. A. Greenberg, K. Jin, Notch-1 signalling is activated in brain arteriovenous malformations in humans. *Brain* **132**, 3231–3241 (2009).
6. D. Delev, A. Pavlova, A. Grote, A. Boström, A. Höllig, J. Schramm, R. Fimmers, J. Oldenburg, M. Simon, NOTCH4 gene polymorphisms as potential risk factors for brain arteriovenous malformation development and hemorrhagic presentation. *J. Neurosurg.* **126**, 1552–1559 (2017).
7. M. Amyere, N. Revencu, R. Helaers, E. Pairet, E. Baselga, M. Cordisco, W. Chung, J. Dubois, J. P. Lacour, L. Martorell, J. Mazereeuw-Hautier, R. E. Pyeritz, D. J. Amor, A. Bisdorff, F. Blei, H. Bombei, A. Dompmartin, D. Brooks, J. Dupont, M. A. González-Enseñat, I. Frieden, M. Gérard, M. Kvarnung, A. K. Hanson-Kahn, L. Hudgins, C. Léauté-Labrèze, C. McCuaig, D. Metry, P. Parent, C. Paul, F. Petit, A. Phan, I. Quere, A. Salhi, A. Turner, P. Vabres, A. Vicente, O. Wargon, S. Watanabe, L. Weibel, A. Wilson, M. Willing, J. B. Mulliken, L. M. Boon, M. Vikkula, Germline loss-of-function mutations in EPHB4 cause a second form of capillary malformation-arteriovenous malformation (CM-AVM2) deregulating RAS-MAPK signaling. *Circulation* **136**, 1037–1048 (2017).
8. S. I. Nikolaev, S. Vetiska, X. Bonilla, E. Boudreau, S. Jauhiainen, B. Rezai Jahromi, N. Khyzha, P. V. DiStefano, S. Suutarinen, T. R. Kiehl, V. Mendes Pereira, A. M. Herman, T. Krings, H. Andrade-Barazarte, T. Tung, T. Valiante, G. Zadeh, M. Tymianski, T. Rauramaa, S. Ylä-Herttuala, J. D. Wythe, S. E. Antonarakis, J. Frösen, J. E. Fish, I. Radovanovic, Somatic activating KRAS mutations in arteriovenous malformations of the brain. *N. Engl. J. Med.* **378**, 250–261 (2018).
9. B. Larrivée, C. Prahst, E. Gordon, R. del Toro, T. Mathivet, A. Duarte, M. Simons, A. Eichmann, ALK1 signaling inhibits angiogenesis by cooperating with the Notch pathway. *Dev. Cell* **22**, 489–500 (2012).
10. T. R. Carlson, Y. Yan, X. Wu, M. T. Lam, G. L. Tang, L. J. Beverly, L. M. Messina, A. J. Capobianco, Z. Werb, R. Wang, Endothelial expression of constitutively active Notch4 elicits reversible arteriovenous malformations in adult mice. *Proc. Natl. Acad. Sci. U.S.A.* **102**, 9884–9889 (2005).
11. H. Cuervo, C. M. Nielsen, D. A. Simonetto, L. Ferrell, V. H. Shah, R. A. Wang, Endothelial notch signaling is essential to prevent hepatic vascular malformations in mice. *Hepatology* **64**, 1302–1316 (2016).
12. D. Miniati, E. B. Jelin, J. Ng, J. Wu, T. R. Carlson, X. Wu, M. R. Looney, R. A. Wang, Constitutively active endothelial Notch4 causes lung arteriovenous shunts in mice. *Am. J. Physiol. Lung Cell. Mol. Physiol.* **298**, L169–L177 (2010).
13. P. A. Murphy, T. N. Kim, L. Huang, C. M. Nielsen, M. T. Lawton, R. H. Adams, C. B. Schaffer, R. A. Wang, Constitutively active Notch4 receptor elicits brain arteriovenous malformations through enlargement of capillary-like vessels. *Proc. Natl. Acad. Sci. U.S.A.* **111**, 18007–18012 (2014).

14. P. A. Murphy, M. T. Lam, X. Wu, T. N. Kim, S. M. Vartanian, A. W. Bollen, T. R. Carlson, R. A. Wang, Endothelial Notch4 signaling induces hallmarks of brain arteriovenous malformations in mice. *Proc. Natl. Acad. Sci. U.S.A.* **105**, 10901–10906 (2008).
15. C. M. Nielsen, H. Cuervo, V. W. Ding, Y. Kong, E. J. Huang, R. A. Wang, Deletion of Rbpj from postnatal endothelium leads to abnormal arteriovenous shunting in mice. *Development* **141**, 3782–3792 (2014).
16. I. Sörensen, R. H. Adams, A. Gossler, DLL1-mediated Notch activation regulates endothelial identity in mouse fetal arteries. *Blood* **113**, 5680–5688 (2009).
17. N. Villa, L. Walker, C. E. Lindsell, J. Gasson, M. L. Iruela-Arispe, G. Weinmaster, Vascular expression of Notch pathway receptors and ligands is restricted to arterial vessels. *Mech. Dev.* **108**, 161–164 (2001).
18. C. Roca, R. H. Adams, Regulation of vascular morphogenesis by Notch signaling. *Genes Dev.* **21**, 2511–2524 (2007).
19. M. J. Cipolla, in *The Cerebral Circulation* (Morgan & Claypool Life Sciences, San Rafael CA, 2009).
20. H. J. Knot, M. T. Nelson, Regulation of arterial diameter and wall [Ca^{2+}] in cerebral arteries of rat by membrane potential and intravascular pressure. *J. Physiol.* **508**, 199–209 (1998).
21. F. M. Faraci, J. E. Brian Jr., Nitric oxide and the cerebral circulation. *Stroke* **25**, 692–703 (1994).
22. U. Förstermann, T. Münzel, Endothelial nitric oxide synthase in vascular disease: From marvel to menace. *Circulation* **113**, 1708–1714 (2006).
23. U. Förstermann, W. C. Sessa, Nitric oxide synthases: Regulation and function. *Eur. Heart J.* **33**, 829–837 (2012).
24. A. U. Syed, G. R. Reddy, D. Ghosh, M. P. Prada, M. A. Nystoriak, S. Morotti, E. Grandi, P. Sirish, N. Chiamvimonvat, J. W. Hell, L. F. Santana, Y. K. Xiang, M. Nieves-Cintrón, M. F. Navedo, Adenylyl cyclase 5–generated cAMP controls cerebral vascular reactivity during diabetic hyperglycemia. *J. Clin. Invest.* **129**, 3140–3152 (2019).
25. M. Schleicher, J. Yu, T. Murata, B. Derakhshan, D. Atochin, L. Qian, S. Kashiwagi, A. Di Lorenzo, K. D. Harrison, P. L. Huang, W. C. Sessa, The Akt1-eNOS axis illustrates the specificity of kinase-substrate relationships in vivo. *Sci. Signal.* **2**, ra41 (2009).
26. O. Augusto, D. F. Trindade, E. Linares, S. M. Vaz, Cyclic nitroxides inhibit the toxicity of nitric oxide-derived oxidants: Mechanisms and implications. *An. Acad. Bras. Cienc.* **80**, 179–189 (2008).
27. D. A. D. Silva, T. M. L. Correia, R. Pereira, R. A. A. da Silva, O. Augusto, R. F. Queiroz, Tempol reduces inflammation and oxidative damage in cigarette smoke-exposed mice by decreasing neutrophil infiltration and activating the Nrf2 pathway. *Chem. Biol. Interact.* **329**, 109210 (2020).
28. A. Samuni, J. B. Mitchell, W. DeGraff, C. M. Krishna, U. Samuni, A. Russo, Nitroxide SOD-mimics: Modes of action. *Free Radic. Res. Commun.* **12**, 187–194 (1991).
29. J. Zielonka, A. Sikora, R. Podsiadly, M. Hardy, B. Kalyanaraman, Identification of peroxynitrite by profiling oxidation and nitration products from mitochondria-targeted arylboronic acid. *Methods Mol. Biol.* **2275**, 315–327 (2021).
30. J. P. Gaut, J. Byun, H. D. Tran, W. M. Lauber, J. A. Carroll, R. S. Hotchkiss, A. Belaaouaj, J. W. Heinecke, Myeloperoxidase produces nitrating oxidants in vivo. *J. Clin. Invest.* **109**, 1311–1319 (2002).
31. T. D. Oury, L. Tatro, A. J. Ghio, C. A. Piantadosi, Nitration of tyrosine by hydrogen peroxide and nitrite. *Free Radic. Res.* **23**, 537–547 (1995).
32. C. J. van Dalen, C. C. Winterbourn, R. Senthilmohan, A. J. Kettle, Nitrite as a substrate and inhibitor of myeloperoxidase. Implications for nitration and hypochlorous acid production at sites of inflammation. *J. Biol. Chem.* **275**, 11638–11644 (2000).
33. M. Toporsian, R. Gros, M. G. Kabir, S. Vera, K. Govindaraju, D. H. Eidelman, M. Husain, M. Letarte, A role for endoglin in coupling eNOS activity and regulating vascular tone revealed in hereditary hemorrhagic telangiectasia. *Circ. Res.* **96**, 684–692 (2005).
34. C. M. Quick, T. Hashimoto, W. L. Young, Lack of flow regulation may explain the development of arteriovenous malformations. *Neurol. Res.* **23**, 641–644 (2001).
35. M. M. Orlich, R. Diéguez-Hurtado, R. Muehlfriedel, V. Sothilingam, H. Wolburg, C. E. Oender, P. Woelffing, C. Betsholtz, K. Gaengel, M. Seeliger, R. H. Adams, A. Nordheim, Mural cell SRF controls pericyte migration, vessel patterning and blood flow. *Circ. Res.* **131**, 308–327 (2022).
36. T. A. Longden, F. Dabertrand, M. Koide, A. L. Gonzales, N. R. Tykocki, J. E. Brayden, D. Hill-Eubanks, M. T. Nelson, Capillary K^+-sensing initiates retrograde hyperpolarization to increase local cerebral blood flow. *Nat. Neurosci.* **20**, 717–726 (2017).
37. P. L. Huang, Z. Huang, H. Mashimo, K. D. Bloch, M. A. Moskowitz, J. A. Bevan, M. C. Fishman, Hypertension in mice lacking the gene for endothelial nitric oxide synthase. *Nature* **377**, 239–242 (1995).
38. T. Aoki, M. Nishimura, H. Kataoka, R. Ishibashi, K. Nozaki, S. Miyamoto, Complementary inhibition of cerebral aneurysm formation by eNOS and nNOS. *Lab. investig.* **91**, 619–626 (2011).
39. W. Meng, J. Ma, C. Ayata, H. Hara, P. L. Huang, M. C. Fishman, M. A. Moskowitz, ACh dilates pial arterioles in endothelial and neuronal NOS knockout mice by NO-dependent mechanisms. *Am. J. Physiol.* **271**, H1145–H1150 (1996).
40. A. Papapetropoulos, K. M. Desai, R. D. Rudic, B. Mayer, R. Zhang, M. P. Ruiz-Torres, G. García-Cardeña, J. A. Madri, W. C. Sessa, Nitric oxide synthase inhibitors attenuate transforming-growth-factor-beta 1-stimulated capillary organization in vitro. *Am. J. Pathol.* **150**, 1835–1844 (1997).
41. C. S. Wilcox, Effects of tempol and redox-cycling nitroxides in models of oxidative stress. *Pharmacol. Ther.* **126**, 119–145 (2010).
42. A. Drouin, N. Thorin-Trescases, E. Hamel, J. R. Falck, E. Thorin, Endothelial nitric oxide synthase activation leads to dilatory H2O2 production in mouse cerebral arteries. *Cardiovasc. Res.* **73**, 73–81 (2007).
43. E. P. Wei, H. A. Kontos, J. S. Beckman, Mechanisms of cerebral vasodilation by superoxide, hydrogen peroxide, and peroxynitrite. *Am. J. Physiol.* **271**, H1262–H1266 (1996).
44. A. C. Chang, Y. Fu, V. C. Garside, K. Niessen, L. Chang, M. Fuller, A. Setiadi, J. Smrz, A. Kyle, A. Minchinton, M. Marra, P. A. Hoodless, A. Karsan, Notch initiates the endothelial-to-mesenchymal transition in the atrioventricular canal through autocrine activation of soluble guanylyl cyclase. *Dev. Cell* **21**, 288–300 (2011).
45. F. Cheng, R. Nussinov, KRAS activating signaling triggers arteriovenous malformations. *Trends Biochem. Sci.* **43**, 481–483 (2018).
46. H. Xu, R. Huo, H. Li, Y. Jiao, J. Weng, J. Wang, Z. Yan, J. Zhang, S. Zhao, Q. He, Y. Sun, S. Wang, Y. Cao, KRAS mutation-induced EndMT of brain arteriovenous malformation is mediated through the TGF-β/BMP-SMAD4 pathway. *Stroke Vasc Neurol.*, svn-2022-001700 (2022).
47. T. Hong, Y. Yan, J. Li, I. Radovanovic, X. Ma, Y. W. Shao, J. Yu, Y. Ma, P. Zhang, F. Ling, S. Huang, H. Zhang, Y. Wang, High prevalence of KRAS/BRAF somatic mutations in brain and spinal cord arteriovenous malformations. *Brain* **142**, 23–34 (2019).
48. Y. H. Kim, H. Hu, S. Guevara-Gallardo, M. T. Lam, S. Y. Fong, R. A. Wang, Artery and vein size is balanced by Notch and ephrin B2/EphB4 during angiogenesis. *Development* **135**, 3755–3764 (2008).
49. E. G. Shesely, N. Maeda, H. S. Kim, K. M. Desai, J. H. Krege, V. E. Laubach, P. A. Sherman, W. C. Sessa, O. Smithies, Elevated blood pressures in mice lacking endothelial nitric oxide synthase. *Proc. Natl. Acad. Sci. U.S.A.* **93**, 13176–13181 (1996).
50. R. Jiang, S. Wang, K. Takahashi, H. Fujita, C. R. Fruci, M. D. Breyer, R. C. Harris, T. Takahashi, Generation of a conditional allele for the mouse endothelial nitric oxide synthase gene. *Genesis* **50**, 685–692 (2012).
51. M. E. Pitulescu, I. Schmidt, R. Benedito, R. H. Adams, Inducible gene targeting in the neonatal vasculature and analysis of retinal angiogenesis in mice. *Nat. Protoc.* **5**, 1518–1534 (2010).
52. M. A. Nystoriak, M. Nieves-Cintrón, P. J. Nygren, S. A. Hinke, C. B. Nichols, C. Y. Chen, J. L. Puglisi, L. T. Izu, D. M. Bers, M. L. Dell'acqua, J. D. Scott, L. F. Santana, M. F. Navedo, AKAP150 contributes to enhanced vascular tone by facilitating large-conductance Ca^{2+}–activated K^+ channel remodeling in hyperglycemia and diabetes mellitus. *Circ. Res.* **114**, 607–615 (2014).
53. M. A. Nystoriak, K. P. O'Connor, S. K. Sonkusare, J. E. Brayden, M. T. Nelson, G. C. Wellman, Fundamental increase in pressure-dependent constriction of brain parenchymal arterioles from subarachnoid hemorrhage model rats due to membrane depolarization. *Am. J. Physiol. Heart Circ. Physiol.* **300**, H803–H812 (2011).
54. P. A. Murphy, T. N. Kim, G. Lu, A. W. Bollen, C. B. Schaffer, R. A. Wang, Notch4 normalization reduces blood vessel size in arteriovenous malformations. *Sci. Transl. Med.* **4**, 117ra118 (2012).
55. Y. Lin, W. Jiang, J. Ng, A. Jina, R. A. Wang, Endothelial ephrin-B2 is essential for arterial vasodilation in mice. *Microcirculation* **21**, 578–586 (2014).
56. S. A. Austin, A. V. Santhanam, Z. S. Katusic, Endothelial nitric oxide modulates expression and processing of amyloid precursor protein. *Circ. Res.* **107**, 1498–1502 (2010).
57. J. Zielonka, J. Vasquez-Vivar, B. Kalyanaraman, Detection of 2-hydroxyethidium in cellular systems: A unique marker product of superoxide and hydroethidine. *Nat. Protoc.* **3**, 8–21 (2008).
58. J. Zielonka, M. Zielonka, B. Kalyanaraman, HPLC-based monitoring of oxidation of hydroethidine for the detection of NADPH oxidase-derived superoxide radical anion. *Methods Mol. Biol.* **1982**, 243–258 (2019).
59. A. Sikora, J. Zielonka, K. Dębowska, R. Michalski, R. Smulik-Izydorczyk, J. Pięta, R. Podsiadły, A. Artelska, K. Pierzchała, B. Kalyanaraman, Boronate-based probes for biological oxidants: A novel class of molecular tools for redox biology. *Front. Chem.* **8**, 580899 (2020).
60. J. Zielonka, M. Zielonka, L. VerPlank, G. Cheng, M. Hardy, O. Ouari, M. M. Ayhan, R. Podsiadły, A. Sikora, J. D. Lambeth, B. Kalyanaraman, Mitigation of NADPH oxidase 2 activity as a strategy to inhibit peroxynitrite formation. *J. Biol. Chem.* **291**, 7029–7044 (2016).

Acknowledgments: We thank C. M. Nielsen for helpful discussions and C. Liu for assistance with line profile measurements for in vivo arteriolar tone. The LC-MS analyses of the redox

probes and oxidation products were performed in Medical College of Wisconsin Cancer Center Redox and Bioenergetics Shared Resource. **Funding:** This work was supported by National Institutes of Health (NIH) NS067420, HL075033, and NS113429; Vascular Cures (formerly the Pacific Vascular Research Foundation); the Frank A. Campini Foundation; the Mildred V Strouss Charitable Trust; American Heart Association (AHA) grant-in-aid 10GRNT4170146 and GRNT 16850032; The Tobacco-Related Disease Research Program (TRDRP) funds 28IR-0067 to R.A.W.; AHA 15POST25110016 Postdoctoral Fellowship to L.H.; and NIH R01HL149127, R01HL161872, and R01HL121059 to M.F.N. and NIH HL142710 to M.A.N. **Author contributions:** Conceptualization: R.A.W. Investigation: L.H., F.C., X.Z., M.A.N., M.J., J. Zielonka, W.X., K.R., S.W., W.J., A.L., K.S.H., J. Zhang, X.W., and A.U.S. Methodology: L.H., F.C., R.A.W., J. Zielonka, X.Z., M.A.N., M.F.N., K.R., W.J., and T.T. Formal analysis L.H., F.C., X.Z., M.A.N., W.X., K.R., A.L., S.Y., S.W., A.U.S., W.J., M.F.N., K.S.H., and J. Zhang. Visualization: L.H., F.C., R.A.W., X.Z., M.A.N., M.F.N., K.R., and A.L. Writing (original draft): L.H., R.A.W., and F.C. Writing (review and editing): R.A.W., L.H., F.C., J. Zielonka, M.A.N., M.F.N., X.Z., T.T., and A.L. Validation: R.A.W., L.H., F.C., X.Z., J. Zielonka, M.F.N., M.A.N., W.X., K.R., S.Y., and A.L. Data curation: L.H., R.A.W, M.A.N., and M.F.N. Resources: T.T. Funding acquisition: R.A.W., L.H., and M.F.N. Supervision: R.A.W. and M.F.N. Project administration: R.A.W. **Competing interests:** The authors declare that they have no competing interests. **Data and materials availability:** All data needed to evaluate the conclusions in the paper are present in the paper and/or the Supplementary Materials.

Submitted 11 September 2022
Accepted 20 April 2023
Published 26 May 2023
10.1126/sciadv.ade7280